Time-Resolved Analysis of Circulation Control over Supercritical Airfoil using Digital Particle Image Velocimetry (DPIV)

Mian M. Hussain

Thesis submitted to the faculty of the Virginia Polytechnic Institute and State University in partial fulfillment of the requirements for the degree of

Master of Science

In

Mechanical Engineering

Dr. Pavlos P. Vlachos, Chairperson

Dr. Demetri P. Telionis, Member

Dr. Clinton L. Dancey, Member

December 15th, 2004

Blacksburg, VA

Keywords: Circulation Control Wing (CCW), Coanda Effect, DPIV, Flow Control, Flow Visualization, Jet Pulsation, Vortex Formation

Time-Resolved Analysis of Circulation Control over Supercritical Airfoil using Digital Particle Image Velocimetry (DPIV)

Mian M. Hussain

ABSTRACT

Active pneumatic flow control methods as applied to aerospace applications have shown noteworthy improvements in lift compared to traditional means. The General Aviation Circulation Control (GACC) concept currently under investigation at NASA's Langley Research Center (LaRC) is an attempt at addressing some of the fundamental obstacles related to the successful development and implementation of such techniques. The primary focus of research in the field of high lift pneumatic devices is to investigate ways of obtaining significant improvements in the lift coefficient without resorting to moving surfaces. Though it has been demonstrated that the lift coefficient can be amplified in a variety of ways, the chosen method for the current work is via enhanced circulation stemming from a trailing edge Coanda jet. A secondary objective is to reduce the amount energy expenditure used in these pneumatic techniques by implementing time-variant flow.

This paper describes experimental observations of the flow behavior at the trailing edge of a modified water tunnel based supercritical airfoil model that exploits both steady and pulsed Coanda driven circulation control. A total of 10 sets of data, excluding a baseline case of no Coanda jet, were sampled with five cases each for steady and pulsed flow, the latter at a reduced frequency, f^+, of 1. Two cases of equal momentum coefficient but with varying forced frequencies were isolated for further study in an attempt to accurately compare the resultant flow dynamics of each method. All measurements were taken at a zero-lift angle of attack by means of a non-invasive time accurate flow visualization technique (DPIV). Vorticity behavior was investigated using Tecplot® and a MATLAB® program was developed to quantify the Strouhal Number of time-averaged velocity fluctuations moving aft of the Coanda surface for each case.

TABLE OF CONTENTS

LIST OF FIGURES

LIST OF TABLES

ACKNOWLEDGMENTS

First and foremost, I am grateful to الله (God) who blessed me with guidance, good health, and friends that supported me all through this chapter in my life. I thank Him for giving me patience and helping me through all the tough times I've encountered in my five and a half years as an engineering student at Virginia Tech, but especially during the writing of this thesis.

I am indebted to many people whom I have come across in my years in Blacksburg that have been instrumental in the attainment of my goals. Some, however, deserve special thanks. I would like to start off by taking this moment to express my gratitude to Dr. Pavlos Vlachos, or Pavlo as he is better known to all of his students. The time and effort you have put in to the completion of this work makes it more of your accomplishment than it does mine. In spite of your research and academic commitments, you have always kept your door open for me and for that I am forever grateful. I would also like to show my appreciation to both of my graduate committee members, Dr. Demetri Telionis and Dr. Clint Dancey. Your encouragement and insightful comments and suggestions were instrumental in making this work possible. My gratitude also goes to Dr. Gregory S. Jones of NASA's Langley Research Center who not only provided the GACC airfoil model that was the backbone of this experiment, but more importantly gave us the opportunity to perform this work. His expertise in this subject matter and advice contributed greatly in the completion of the effort.

To everyone in the fluids lab, thank you for your support and encouragement. A special thank you goes out to Ali Etebari, José Rullán, Chris Weiland, and John Charonko. I don't think I could have done this without you! I would also like use to this text as a podium to express my gratitude for all those friends that have made my years as a Hokie memorable ones. Throughout time, for better or for worse, true friends are forever.

Furthermore, I am grateful to the Department of Aerospace Engineering and Mechanical Engineering faculty, staff and fellow students who were an indispensable part of my overall learning experience. And last but by no means least, I'd like to thank my parents for their

adamant love and support. I don't think I will ever be able to repay all the sacrifices that you have made for me. This thesis is dedicated to you.

Yet again, all gratitude goes to الله alone…
(El Ham'd el Allah)

Dedicated to my parents,
Without your love and perseverance, I would not be here today…

NOMENCLATURE

α	Angle of Attack
$\bar{c}$	Airfoil Chord
C_μ	Momentum Coefficient
f	Actuator Frequency (also Driver Frequency)
f^+	Reduced Frequency
$f_{shedding}$	Shedding Frequency
h	Slot Width
$\dot{m}$	Mass Flow Rate (of Coanda Jet)
q	Dynamic Pressure (of Freestream)
Re	Reynolds Number (based on Chord)
S	Wingspan
St	Strouhal Number
t	Airfoil Thickness
U_0	Freestream Velocity
U_{jet}	Coanda Jet Velocity (at exit)

CHAPTER 1

1 BACKGROUND AND INTRODUCTION

1.1 Background

The primary objective of Circulation Control (CC) is to increase the circulation around an airfoil in order develop high lift and readily vary lift on command using pneumatic jet actuators so as to eliminate the use of mechanical devices or moving aerodynamic surfaces. Currently, the optimization of aerodynamic characteristics of lifting surfaces is achieved by appropriate design of the airfoil section. The modification of the predetermined shape of the airfoil in an attempt to vary lift and drag is attained using such methods as leading and trailing edge flaps. Unlike mechanical techniques currently utilized for generating lift, the current work offers the benefit of attaining amplification of lift coefficient with no conventional moving surfaces, thereby making it an effective candidate for designs that take into consideration stealth. Coanda based CC is based on introducing a high momentum thin jet tangentially at a rounded trailing edge in the flow with the aim of forcing the fluid around the curved surface at that location. In doing so, the trailing edge stagnation point is moved upstream while the leading edge stagnation point is simultaneously moving downstream hence increasing circulation and consequently augmenting lift. The background theory of this approach can be found in the well-documented Kutta-Joukowski Theorem which explicitly establishes a direct relation between circulation around a body and the net lift acting on that body

1.1.1 Coanda Effect

Present work in the field of high lift augmentation devices is part of an ongoing series of similar studies that place emphasis on active jet actuation flow control for the optimization of lift and drag characteristics of lifting bodies. Among the more successful techniques currently being investigated at NASA's Langley Research Center (LaRC) is a method that involves virtual aerodynamic shape change via pneumatic flow control. This is achieved by ejecting a fluid from within the airfoil in such a way that the external potential flow characteristics are altered creating a virtual airfoil shape. "Circulation Control", is one such technique that makes use of the Coanda effect to increase the lift coefficient via increased circulation. The Coanda effect, named after Dr. Henri Coanda, is the tendency of fluid flow to adhere to a curved surface provided that it does not have to negotiate a sharp turning angle. The current work makes use of this flow property by

utilizing a 2-D jet that exits from a slot tangential to the so-called Coanda surface. The wall bounded jet has a velocity profile similar to that of a laminar boundary layer near the surface but that of a freestream i.e. even velocity distribution, at distances farther from the surface. The amount of turning that the jet can attain is subject to a number of variables, among them the slot height, jet velocity and Coanda surface geometry. When upper surface tangential fluid ejection is applied to a rounded trailing edge of a wing, the normal tendency of the flow to separate at or before the trailing edge is overcome and the flow is carried onto the lower surface. The location of the effective rear stagnation point is moved upstream while the front stagnation point is pushed downstream, thereby allowing the wing to develop additional global circulatory flow, as if the camber of the airfoil has increased (see Figure 1.1.1.1). Active flow control takes advantage of the sensitivity of lift to flow conditions at the trailing edge. In certain circumstances, the flow can be directed downward or even in the opposite direction i.e. a Coanda turning angle of 180º. Specifically, it is the resulting stability between the centrifugal force around the Coanda surface and the sub-ambient pressure in the jet sheet that is responsible for the adherence of the jet to the curved surface.

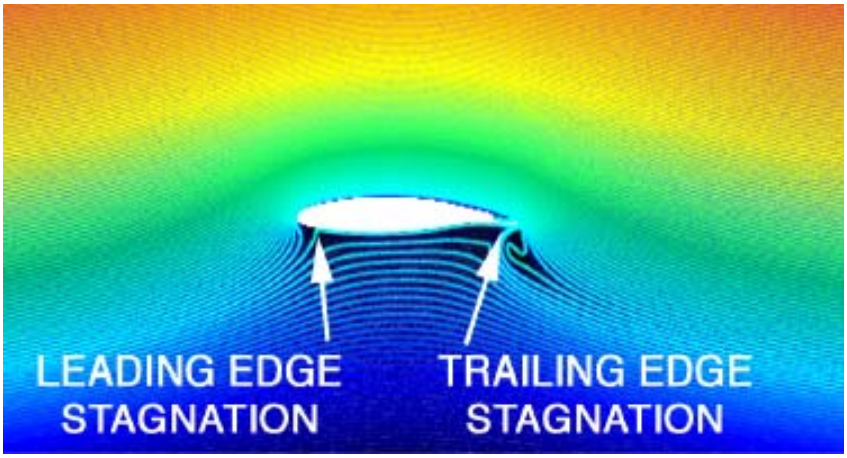

Figure 1.1.1.1 – CFD illustration of variation in stagnation point location as a result of Coanda jet (Jones et al., 2002)

Though the potential applications of a Coanda jet include an effective form of boundary layer control, our interest in this idea stems from its ability to increase circulation around the airfoil. Kutta (1902) and Joukowski (1911) are accredited with being the first to quantitatively relate the net lift acting on a wing to the integration (closed form) of the velocity field along a streamline. This mathematical equality which relates circulation, denoted by "Γ" to lift, is shown

in Figure 1.1.1.2. A schematic that illustrates the effect that circulation can have on the lift acting on a symmetric body (which would otherwise have no lift component) is shown in Figure 1.1.1.3. Note that the application of an angular velocity component acts to increase circulation by bringing the stagnation points at the pressure side (bottom in the figure) closer together.

$$\Gamma = \oint V \cdot dL$$

$$Lift = \rho \cdot U \cdot \Gamma$$

Figure 1.1.1.2 – Mathematical relation between circulation & the integral of velocity field (top) and lift & circulation (bottom)

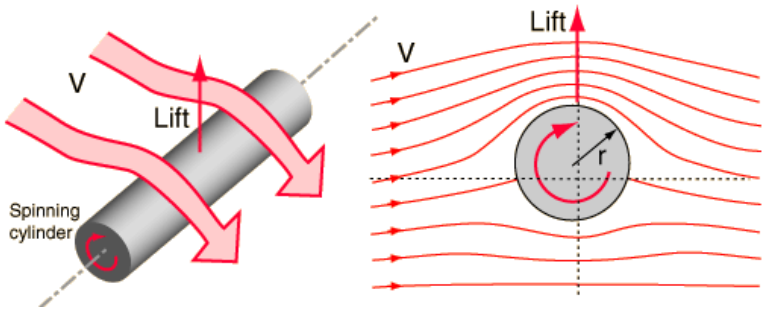

Figure 1.1.1.3 – Schematic illustrating the effect of rotation in amplifying lift on a symmetric body

Upon exiting the slot, the Coanda jet will interact with the flow field in such a way that the streamlines are pushed farther down thereby creating "virtual camber". The result of this interaction in the behavior of the flow is comparable with that resulting from mechanical high lift systems such as flaps. In addition to creating virtual camber, the jet also acts to force the rear stagnation point closer toward the leading edge while simultaneously pushing the leading edge stagnation point backwards. Provided that the Coanda jet has a high enough momentum, the two stagnation points can be forced so close to one another that they form a singularity point. Assuming that the thrust effects are ignored, such a configuration would translate to a lift coefficient as high as 4π.

1.1.2 Flow Control Methodologies

The roots of flow control and its relevant applications can be traced back to Prandtl who is credited with being the first to introduce boundary layer theory and explain the mechanics of steady flow separation. In his landmark presentation to the Third International Congress of Mathematics at Heidelberg, Germany in 1905, he described a number of experiments where he was able to control the boundary layer using what would be regarded as somewhat primitive active flow control techniques by today's standards. Typically, the aim of employing a flow control technique as applied from an aerodynamics standpoint is to enhance lift, reduce drag, and suppress noise resulting from pressure fluctuations within a flow, though usually a combination of the aforementioned as demonstrated in Figure 1.1.2.1. Part of the challenge in attempting to develop an effective means of carrying out the tasks mentioned above stems from the high costs that are usually associated with the implementation of new techniques. It is vital that in the process of developing alternative methods designed to save fuel over the long run, emphasis is placed on minimizing operation and maintenance costs as ignoring these has the potential to render the project obsolete from an economical perspective.

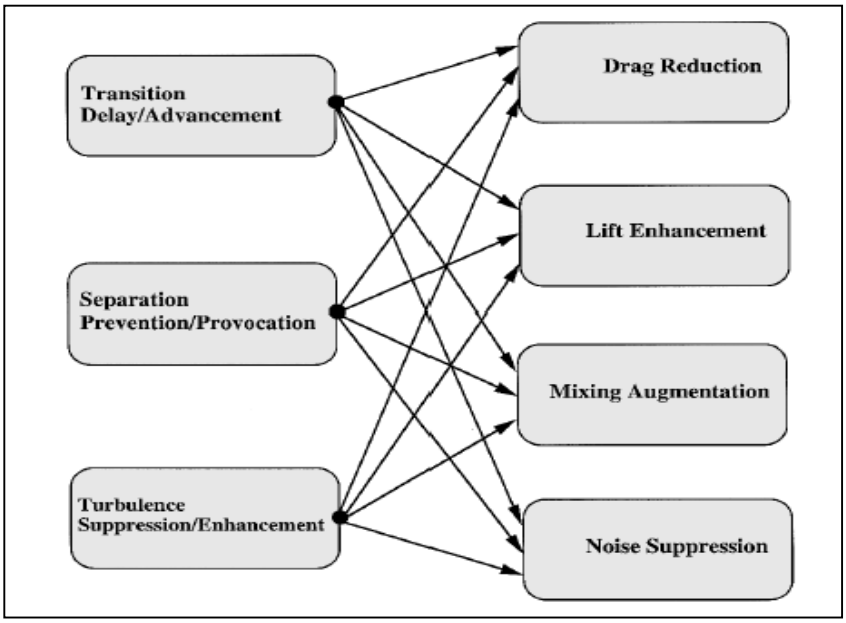

Figure 1.1.2.1 - Classification of flow control techniques for various aerodynamic objectives (Gad-el-Hak, 2001)

Since the days of Prandtl's revolutionary paper, a variety of distinct forms of flow control have undergone investigation and many derivatives of this technique have been developed. The various types of techniques currently being investigated can be broken down into two broad categories: passive and active flow control, the latter consisting of either predetermined flow control or reactive flow control (see Figure 1.1.2.2). The distinction between predetermined and reactive flow control stems from the ability of reactive flow control to modify the response to a flow condition resulting from the immediate condition of the flow (based on some form of direct measurement) whereas the former is based on the application of energy input with disregard to the state of the flow at the given instance.

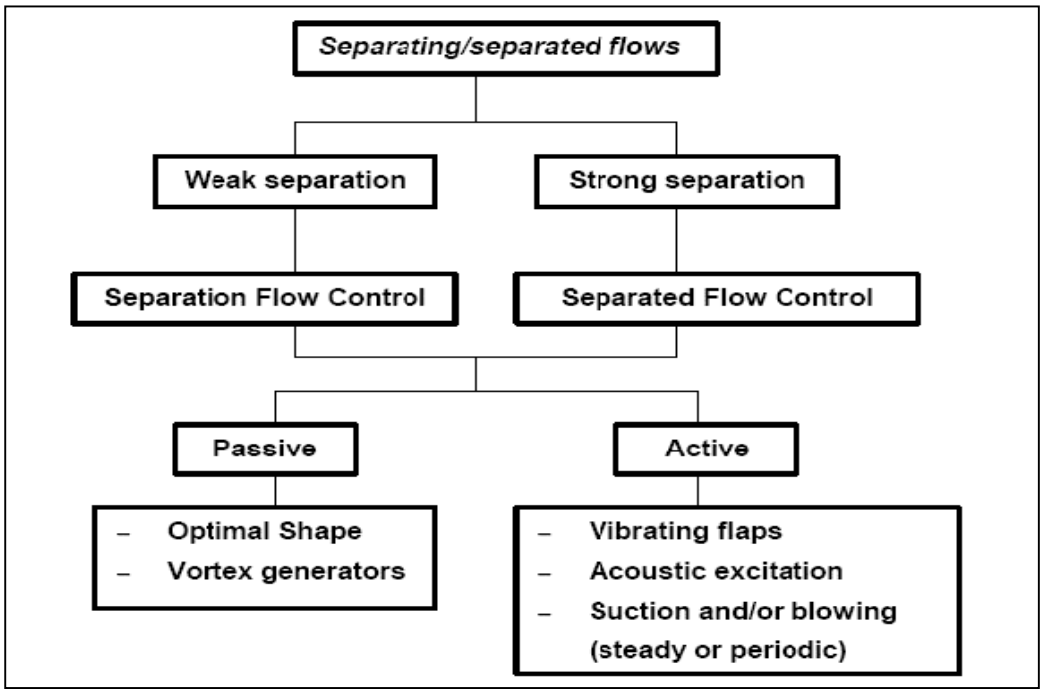

Figure 1.1.2.2 - Classification of flow field separation and flow management techniques (Fiedler et al., 1998)

Despite the promise illustrated by Prandtl's revolutionary findings, very little progress was made in this branch of aerodynamics in the years leading up to World War II. Extensive research findings were undertaken by Germany during the course of the Second World War in an attempt to expand on the technical knowledge available in aerodynamics at the time. This trend continued at the end of World War II with the United States leading the way with extensive research on laminar flow control. The predominant focus of this work lied in developing

techniques such as boundary layer suction where keeping flow in a laminar state, especially at transonic mach numbers, was heavily emphasized. Added incentive to develop novel methods for lift enhancement and drag reduction came in the early 1970s in the form of an oil crisis along with a rapid growth in the airline industry. Over the course of the past decade, military applications including both aeronautical and naval, have been at the forefront of development for research in this area.

In addition to boundary layer suction as a means of maintaining laminar flow at transitional Reynolds's numbers, significant research in the past sixty years has been conducted in an effort to control and delay the separation of flows over lifting surfaces. Unlike the goal of boundary layer suction, the predominant objective in such techniques is not to reduce drag but rather to improve aerodynamic performance at high angles of attack and extend the flight envelope.

1.2 Testing Techniques

1.2.1 Experimental Measurement Techniques

Generally speaking, pneumatic actuation as a method of flow control can be broadly categorized into two areas. Time-invariant actuation (steady) where fluid passes through a surface boundary at a constant rate was one of the first to be developed. This category of fluid actuation can involve either continuous blowing (e.g. Attinello) or suction (e.g., Chang). Due to the temporally invariant nature of this technique, significantly greater mass flux is required in order to attain the same amount of effectiveness as temporally variant i.e. pulsed techniques. An extensive amount of research has been conducted over the course of the past twenty years with the objective of determining how the same level of efficacy can be obtained by using less mass flux or alternatively using the same mass flux via temporally invariant pulsing in order to obtain greater levels of effectiveness. It has been shown that pulsed blowing (e.g., Seifert, 2000) offers a means of increasing the lift coefficient at a given mass flux rate. The present work is an attempt to analyze the flow physics at a rounded trailing edge for both continuous and time variant cases with fewer emphasis placed on the effect that different flow rates have on the net lift.

Fluidic modification of the apparent aerodynamic shape of an airfoil has utilized active flow control techniques such as the one this paper intends to address in both attached flow that is near the point of separation as well as flow that is already separated. In the case of the former, Smith et al. (1998) and Amitay et al. (1998, 1999) demonstrated the utility of synthetic zero mass flux jet actuators. In addition to delaying flow separation, the authors were able to successfully enhance the lift and reduce the pressure drag. The authors used actuation frequencies that were an order of magnitude higher than the natural frequency of the flow over the airfoil. Their work points to the interaction between high-frequency zero net mass flux jets and the local flow, in particular the partial or full reattachment of flow, as the cause of modification of the apparent aerodynamic shape. Furthermore, the authors point to the location and the effectiveness of the actuators as the primary factors in determining the degree of attachment. It was also suggested by the authors that the actuators could be effective in either side of the airfoil including locations upstream of the separation point. In their attempt to investigate the effect of actuator frequency and momentum coefficient on the interaction domain, Amitay and Glezer (1999) show that the quasi-steady lift coefficient of the reattached flow can be amplified by means of a time variant input that would lead to a narrower wake. In both of the above cases, the intention of the authors was to explore a way in which flow over the suction side of the airfoil that is nearing separation could be reattached, either partially or fully. Note that the emphasis on the latter work is based almost entirely on the ability of flow at high angles of attack to provide a large lift coefficient whereas the subject of the current work places more emphasis on attaining the same goal by means of increasing circulation. The use of a jet at the trailing edge, which will be discussed in more detail later in the course of this paper, allows for the presence of a net lifting force even at zero lift angles of attack.

Conventionally the camber modification of the flow around an airfoil can also be achieved using mechanical means. In such a case, a variety of techniques have been suggested including a rotating cylinder (e.g. Modi, 1988) and an oscillating fence (e.g. Urzynicok, 2002). Like the jet actuators discussed earlier, a rotating cylinder serves to inject momentum into the boundary layer by exploiting the “no slip” condition present at the surface which serves to effectively input momentum into the trailing edge. Modi et al. suggest that the application of a rotating cylinder on a symmetric airfoil can not only delay stall by nearly 50º, but can also

amplify the lift by as much as a factor of two. The work of Urzynicok et al. on the other hand suggests that the implementation of an oscillating cylinder along the entire span of a Wortmann FX 61-164 laminar glider can enhance lift by up to 40%. It is noteworthy to mention at this point that in the case of a rotating cylinder, the authors are able to generate greater circulation by providing a velocity component to the wall itself which in turn forces the flow around the trailing edge. This is somewhat analogous to the technique which will be discussed in the current work. Unlike these previous efforts, our goal is to attain circulation increase by providing momentum to the fluid not by a mechanical device but rather by direct momentum input to the fluid itself by means of both a steady as well as an unsteady jet.

A wide variety of flow control methods have already been successfully implemented in practical engineering devices. Postponement of flow transition from laminar to turbulent and preventing separation can be accomplished using a combination of both passive and active control strategies, some of have already been mentioned. Reviews of such classical techniques include, but are not limited to, works by Bushnell (1983, 1994), Wilkinson et al. (1988), Bushnell and McGinley (1989), Gad-el-Hak (1989, 2000), Bushnell and Hefner (1990), Fiedler and Fernholz (1990), Gad-el-Hak and Bushnell (1991), Barnwell and Hussaini (1992), Viswanath (1995), and Joslin et al (1996). The emphasis that these works place is in the development of techniques to delay laminar-to-turbulence transition. Despite extensive research conducted in this field, serious limitations still exist when transitioning from the laboratory to real life applications. Energy considerations, namely the penalty associated with the control device in attempting to manipulate the flow over a body has to be less than the savings resulting from its use. This need for economically feasible solutions to achieve control is the predominant factor inhibiting their implementation in aerospace applications Though the current work does not focus on ways to reduce energy expenditure, it is nevertheless important that this be kept in mind when exploring alternative practices.

In addition to research intended to investigate the lift and drag behavior of airfoils with the use of actuators, studies have also been carried to analyze flow behavior. Work by Amitay (2002) in the role that actuator frequencies play in fluid behavior demonstrates that the nature of vortices within a region of separated flow varies considerably with the dimensional frequency of

the actuator. In this particular work, the actuation frequency f+ was varied between O(1) and O(10). The results reveal that when the dimensionless frequency is on the order of one, i.e. f+ = O(1), vortical structures exist at locations significantly aft of the trailing edge. On the other hand, when the actuator frequency was increased by an order of magnitude, a complete reattachment of flow with absence of vortical structures was observed. These observations point to the possibility that higher order actuator frequencies can lead to a complete flow reattachment. Not surprisingly, similar work in the field of diffuser flow by the same author points to nearly identical results for internal flow. Unlike flow over an airfoil, however, it was revealed that synthetic jets can be used to reattach flow that has already been separated. The effects of jet actuation frequency and momentum coefficient by the same authors were also studied in an attempt to better understand flow behavior in the interaction domain. Results indicate that though dimensionless frequencies on the order of 10 are conductive to drag reduction, frequencies an order of magnitude lower i.e. f+ = O(1), actually enhance the drag coefficient. It is noteworthy to mention that these studies were conducted using Particle Image Velocimetry (PIV).

PIV was also utilized by Munday et al. (2002) in order to examine the effects of flow control though the work is focused primarily on the application of flow control as a form of oscillatory camber control. The authors utilized a synthetic actuator placed internally in the suction side of the airfoil in order to examine the effect of the actuator response to camber. The broader goal of this work was to examine whether the modification of wing shape by such means could be an effective form of separation control.

The use of momentum influx as a means of enhancing lift in a Circulation Control Wing (CCW) has been examined in the past by Bradley and Franke (1997). In their work, the dynamic characteristics of a CCW, in particular the lift, drag, and pitching moment characteristics were studied. A 20% thick 8.5% cambered wing with a leading edge nose droop and a trailing edge splitter was placed in a flow with a Reynolds number (based on chord) of 500,000. Results from this experiment show that the leading edge nose droop amplified the stall angle of attack as the momentum coefficient was increased. The most notable achievement of this work was the illustration that by means of momentum injectors, the stall angle of attack of an airfoil could be improved provided a leading edge droop was used in conjunction with momentum influx. The

latter allowed the freestream to negotiate the sharp turn at the leading edge that would otherwise have not been possible without pneumatic implementation. This work illustrates that a jet placed at either the leading edge or trailing edge has the potential to provide benefit though the former has primary usage in delaying the onset of stall at high angles of attack while the latter, which will be discussed more thoroughly over the course of this paper, provides a means of lift augmentation via increased circulation.

Rogers and Donnelly (2004) conduct an investigation to inspect the feasibility of a Coanda-effect circulation control device to low aspect ratio control surfaces such as those found on submarines with the intention of finding a feasible application to high-lift control surfaces for underwater vehicles. The uncambered wing model utilized in the study exploited both upper and lower jet slots thereby allowing for the generation of lift in either direction. The results indicate that the circulation control effects on lift are consistent with those found from an increase in angle of attack. An interesting side note, however, was that flow from the second slot has the potential to improve lift by inhibiting effects resulting from excessive turning at high values of C_{μ}. As expected, the use of both slots in tandem allows for the fusion of both wall-bounded jets into a free planar jet.

Investigations into flow controls have also been conducted by Mitchell et al. (1999) in an attempt to modify the locations of vortex breakdown on the surface of a sharp-edged delta wing placed at high angle of attack. The basic setup used by the authors consisted of a model with jet injection at the trailing edge placed in a water tunnel, a setup very similar to that used in the current work. The amount of jet injection was varied in an attempt to change the leading edge vortex breakdown locations. By using flow visualization techniques in a water tunnel, the authors were able to get a visual description of the strength and natural frequency of leading-edge vortices as well as the breakdown locations. A secondary result that came out of this research was the indication that higher mass flow rates can actually be detrimental for sharp edged airfoils. Specifically, it was shown by Mitchell that high momentum coefficients when used for asymmetric cases resulted in the acceleration of vortex breakdown frequencies. Though the results primarily serve to indicate the potential that trailing edge injection offers for altering

the leading-edge vortex breakdown positions, the work also illustrates the effectiveness of flow visualization techniques in water tunnel experiments to reveal the structure of the flow.

In addition to application for lifting surfaces, a significant amount of research work has also been accomplished in the application of flow control on turbomachinery applications i.e. axial compressors and turbines. Carter et al. (2001) developed and tested a modified high-turning compressor stator utilizing flow control. The design in question utilized both boundary layer suction and blowing for enhancing the wake turning angle. Both the suction and blowing were derived form a single pressure source. For measuring the efficacy of such a technique, the pressure loss was measured experimentally and compared with the baseline case i.e. no flow control. A reduction of 65% from the baseline flow pressure coefficient was achieved by the authors along with an increase in wake turning angle by 4.5º when the mass flow rate of the injectors was the equivalent of 1.6% of the total flow in the passage. Measurements of the pressure loss were the primary indicators of the effectiveness of the design. More recent work in flow control to turbomachinery conducted by McQuilling and Jacob (2003) investigates application of flow control around a low pressure turbine blade. In an attempt to examine transitional behavior, the authors compare steady blowing with pulsed blowing at a variety of frequencies and duty cycles. Results point to a complete elimination of flow separation in almost all cases presented.

Though an extensive amount of research findings are available for low speed flow control applications, the research in pneumatic aerodynamics is not limited to incompressible flow. Hites et al. (1997, 2001) demonstrate for the first time the effectiveness of the oscillatory blowing as a means of separation control for high speed flows. Though these results are based on subsonic Mach numbers (M = 0.3), the flow exhibits compressibility effects. Much like works already discussed, the primary objective of the endeavors was to derive methods for lift enhancement over Mach numbers ranging form M=0.1 to M=0.4. It was noted by the authors that the amplification of the lift coefficient was sensitive to the driven frequency regardless of Mach numbers. However, it was also noted that for higher speed cases, the amplification that could be attained from pulsatile blowing could not be repeated for the steady cases regardless of the amount of mass flux.

Cambers and Jones (2001) conducted research to examine the effects that density variations have on actuator performance. Pressure ranging from 0.27 to 1 atmosphere was used in conjunction with Mach numbers of 0.1 and 0.2. The main finding from this work pointed that lower frequencies increase the strength of the synthetic jets. It was also found that higher velocities near the surface on which the actuators were placed, partially inhibited the performance.

Though the present work explores the potential applications of pneumatic flow controls for low speed airfoils, the implementation of this technique exhibits promise of an equally effective impact for high speed applications. Work by Mavris and Kirby (1999) suggest the possibility of the application of circulation control technology aimed at to a generic High Speed Civil Transport (HSCT). Specifically, emphasis is placed by the authors on the role that synthetic jet actuators would play in the high-lift configuration i.e. take-off and landing of such a project. It was illustrated by the authors that compared to a no flow control reference case, the application of synthetic jet actuators could reduce takeoff length by over 30% by enhancing the lift coefficient through the application of circulation control.

1.2.2 Numerical Techniques

Work done by Joslin et al. (2001) is focused on examining the flow behavior of a Coanda jet using numerical simulations. The authors use a combination of flow control methodologies already in place in conjunction with Direct Numerical Simulation (DNS) for hydrodynamic wall-bounded flows. The techniques used, however, can be applied to a wide variety of flow scenarios including Coanda jets and layers of momentum influx. Additional work by Joslin (2001) focused on examining the degree of applicability of Reynolds-Averaged Navier-Stokes (RANS) techniques for active flow control applications. By utilizing both two- and three-dimensional results, it was proven that in spite of some convergence and grid resolution problems, results obtained by numerical algorithms could be effectively used in place of direct experimental measurements.

Englar et al. (2004) conducted a study in which an unsteady three-dimensional Navier-Stokes algorithm was developed with the specific intention of procuring a numerical technique designed explicitly for Circulation Control Wing configurations. Through the examination of the effects of both steady and pulsed jets in two dimensions on a CCW airfoil, the authors were able to effectively replicate results that have been produced through experimental means. Specifically, it was shown that both steady and unsteady jets can produce lift at zero angle of attack. Additionally, it was shown that unsteady blowing can not only eliminate vortex shedding at the trailing edge but can also be used effectively to reduce energy expenditure. The latter is accomplished by applying a time-variant configuration for the actuators which allows for lower energy consumption in a time-averaged sense.

Research in the application of a Coanda jet on supersonic flow is also under investigation. Using Computational Fluid Dynamics (CFD) analysis, Asami and Sawada (1996) investigate Coanda flow in an underexpanded supersonic environment. Using both 2-D and 3-D Navier-Stokes based algorithms, the authors were able to analyze the behavior of a wall bounded Coanda jet around a circular cylinder, geometry almost identical to the one discussed in the current work. Despite the compressibility effects associated with such high speeds, the authors were able to obtain results that were consistent with those collected by experiments in the case of 2-D flow. Wall effects however, were cited as the driving factor responsible for significant disagreement between numerical and experimental results for the case of effects where the flow had a significant three-dimensional component.

In a similar study, the effect of pressure ratios and nozzle configurations on the behavior of a supersonic Coanda jet is conducted by Kim et al. (2000). Conclusions from this work point to both of the aforementioned variables i.e. nozzle pressure ratios and configurations as the driving factors determining flow behavior. To further examine numerical modeling of a supersonic Coanda jet, Liu et al. (2004) developed an unsteady three-dimensional Navier-Stokes algorithm specifically adapted for Circulation Control Wings (CCWs). Similar work into the effects of Coanda jets in the leading edge of a nacelle by Wu et al. (2004) shows promise for the implementation of this technique for engine inlets. Though the findings do not reveal new flow physics of a Coanda jet, they point to the possibility of using such a technique to spread jet

exhaust velocity. Similar to the work done in the field of zero net mass flux actuators, the work also points to the streamwise location of the jet as a factor determining the flow properties.

1.3 Motivation

The capacity to alter a flowfield to generate a desired behavior using either active or passive flow control techniques has potential that could revolutionize air transport as it is known today. Not only does implementing an economically viable flow control technique have the potential of saving billions of dollars annually in fuel costs but it also paves the way for the development of more economically viable solutions for a myriad of other industry products.

Over the course of the past few years, there has been mounting interest in the application of jets that exploit the Coanda effect for flow control applications. Unlike the majority of contemporary work in the area of flow control applications, the major advantage of such a concept when applied to lifting bodies such as wings lies not in stall delay or drag reduction but rather in lift augmentation via improved circulation. That being said, it is well documented that the application of jets to bluff bodies such as an aircraft fuselage can lead to substantial drag reduction as well. The successful application of such a technique on airliners could dramatically reduce runway length required for take-off and landing thereby opening up thousands of smaller airports around the world currently deemed inadequate for large aircraft. Applied on a smaller scale, this technology holds promise for Personal Aerial Vehicles (PAVE), a concept that could dramatically reduce traffic problems faced today and open up a whole new means of transportation for short distances. Research also indicates that the application of a Coanda jet to turbomachinery components such as engine nacelles, compressors, and turbines holds the promise of significantly improving the performance of these components by altering the behavior of flow to minimize detrimental effects.

1.4 Contribution

A number of circulation control devices that benefit from a high turning angle have been studied both experimentally and analytically. However, the majority of these cases have involved mechanical trailing edge flow control devices i.e. rotating cylinder, as opposed to the pneumatic ones currently being investigated. The current contribution investigates the dynamics of the flow physics at the trailing edge of a circulation control airfoil via both steady and unsteady excitation. In an attempt to amplify the lift coefficient, a jet was forced out of the tangential slot on the suction side (high lift configuration), thereby forcing the rear stagnation point on the pressure side upstream (and hence increasing circulation around the airfoil). The flow physics from this change were analyzed by resolving time-dependent characteristics of the flow.

The current piece is rooted in research that has been conducted by Jones et al. on both steady and unsteady pneumatic flow control as applied to Circulation Control Wings. It must be stressed that the nature of the present work focuses predominantly on the flow physics of a Circulation Control device. As mentioned earlier, a significant deal of work has been done in exploring the benefits of a Coanda surface as applied to a high lift device. There remains, however, a gap in knowledge with regards to the nature of flow behavior when such a device is implemented. The present effort is the first to employ kHz Time Resolved Digital Particle Image Velocimetry to resolve the global characteristics of the flow. Data was collected and analyzed on a supercritical airfoil model placed in a water tunnel. The work focuses on the fluid dynamics at and aft of the Coanda surface and reveals the spatio-temporal evolution of the inherent natural and forced unsteadiness. Comparisons of steady and unsteady blowing and different forcing strengths illustrate for the first time the variations between the different flow condition and their possible ramifications to the efficiency of a Coanda based Circulation control.

CHAPTER 2

2 METHODS AND FACILITIES

2.1 Introduction

The present experiment was conducted in Virginia Tech's Engineering Science and Mechanics (ESM) Fluids Laboratory located in Norris Hall. The GACC model used was provided by Dr. Gregory S. Jones of NASA's Langley Research Center. The various components of the DPIV system used in the completion of this work are described in more detail in this section.

2.2 ESM Water Tunnel

The Engineering Science and Mechanics (ESM) Water Tunnel used for this experiment was designed and built by Engineering Laboratory Design (ELD). The basic design is fabricated of a composite lamination of fiberglass-reinforced plastic and encompasses a closed loop with flow arranged in a vertical configuration with an approximate capacity of 2500 gallons (9500 liters). Schematics of this facility's side view and top view are illustrated in Figures 2.2.1 and 2.2.2 respectively. The overall dimensions of the water tunnel are 8.74m by 2.74m by 2.00m. Among the tunnel components are the flow sections including a return plenum with an incorporated turning system that divides and re-directs the flow aft of the test section. Additional components include a 24 inch return PVC pipe, an inlet plenum, multiple flow straighteners located fore of the test section, and a three-way convergence section with a contraction ratio of 6:1. The test section has dimensions 24" by 24" by 72" and is made of 1¼" clear acrylic plexiglass to allow for clear optical access of the experimental apparatus. Supplementary items worth mentioning are 4500 Gallon/min single stage axial flow pump and a variable speed drive assembly consisting of a 20 hp motor actuated by a variable frequency controller that allows for a precise adjustment of freestream velocity of up to 100 cms^{-1}.

The turbulence intensity and maximum velocity pertaining to flow at the test section are dependent on the volume of fluid in the tunnel. The former variable is contained by a set of screens located in the settling chamber, each with a fine mesh for turbulence reduction and flow straightening. The maximum turbulence levels in the tunnel (corresponding to when it is full) are known to be about 2%. The current study, however, was conducted with the tunnel only partially full and with the upper surface of the fluid free. In order to negate the possibility of an increase

in turbulence levels from vibrations resulting from the pump, rubber couplings were used to adjoin the piping to the flow sections. A turning vane system located within the return plenum is used to direct the flow leaving the test section.

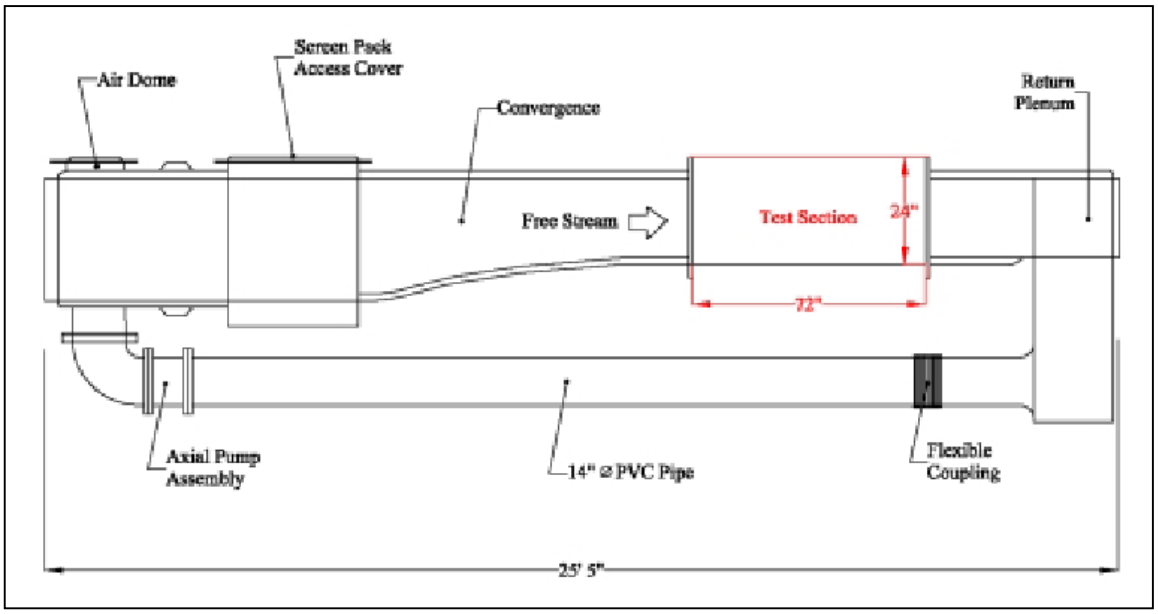

Figure 2.2.1 – Schematic representation of ESM Water Tunnel (Side View)

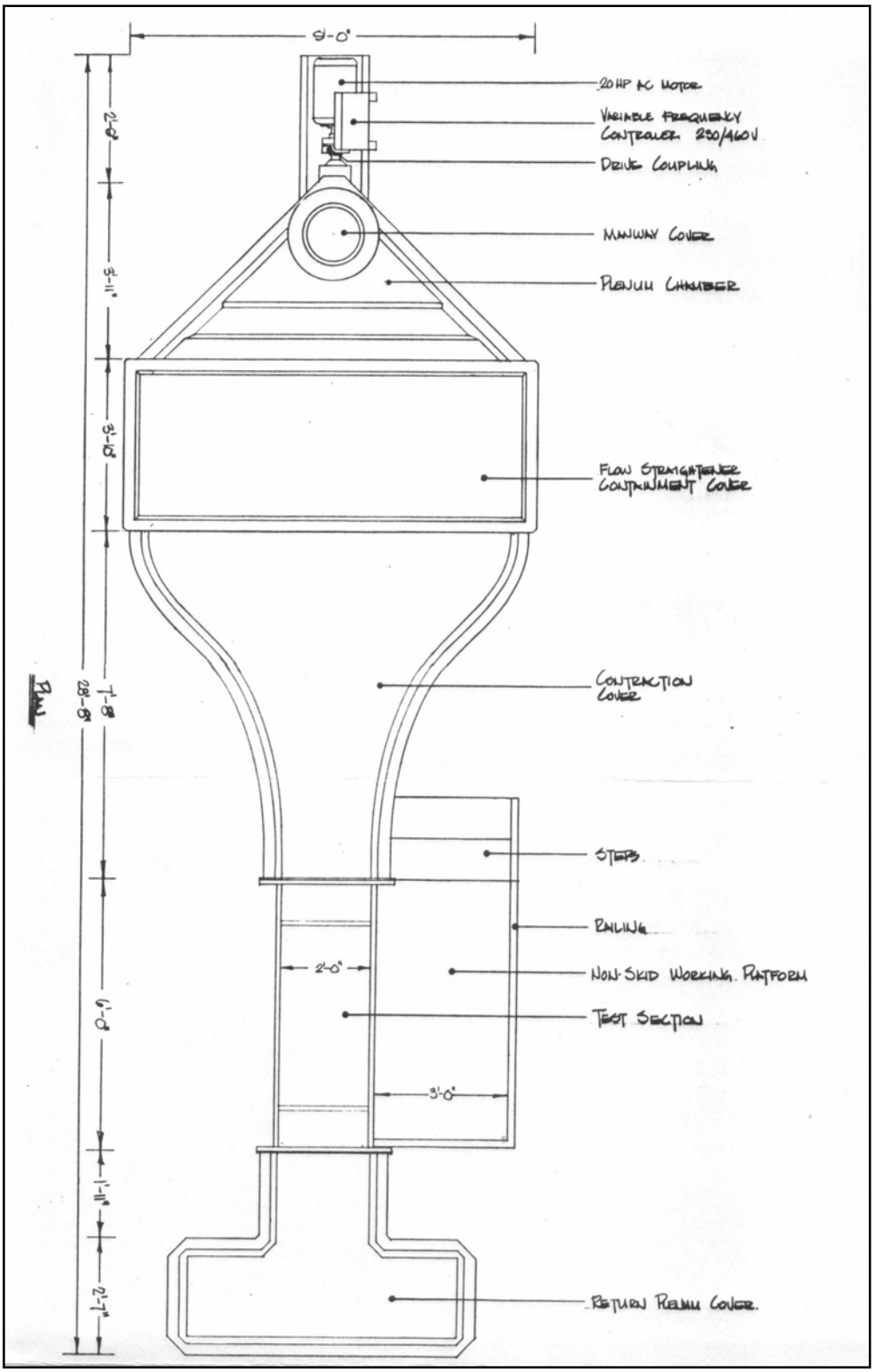

Figure 2.2.2 – Schematic representation of ESM Water Tunnel (Top View)

2.3 Particle Image Velocimetry (PIV) Background Theory

The foundation for Particle Image Velocimetry (PIV) can be traced back to traditional qualitative flow visualization techniques but the present form can be attributed in part to Meynard (1983). The system, however, was not digitalized until the early nineties (Willert and Gharib, 1991), Westerweel (1993a, 1993b) and Huang and Gharib (1993). Current applications of PIV have evolved from very basic ones two decades ago to include a wide array of flows ranging from Micro-PIV for measurements related to bio-medical applications such as capillary flow, for example, to supersonic gas flows.

Emphasis in the digital implementation of the PIV system placed a single exposure, double-frame digital cross-correlation technique as well as the utilization of a high resolution camera with a frame rate of 30 frames per second (fps) or greater thereby resulting in a minimum sampling frequency of 15 Hz . The technical aspects of such a system do not allow for a clear distinction between sizable differences in flow velocities which is one of the benchmarks of such a system. The system that is used in our studies, however, addresses these issues and thereby lays the foundation from which accurate measurements can be made. The most common implementation of this technique integrates a light sheet generated by a pulsating laser used to illuminate the area of interest with a high-resolution CMOS camera. Though the configuration used by the system is subject to variation, the one used for the present study employed 1000 instants of the flow field per second i.e. sampling rate of 1000 Hz. The use of a pulsed laser provides high energy source with good coherence which, when used in conjunction with a CMOS camera (chosen because of a superior signal-to-noise ratio), allows for the delivery of superior spatio-temporal results.

The underlying principles of DPIV essentially state that, by utilizing a high speed video in conjunction with a light source, a flow field can be recorded in a series of images. These images will in turn be used to deduce velocity measurements. The resolution of these spatio-temporal measurements is affected by hardware other than the laser, namely the high speed camera and optics. As illustrated in Figure 2.3.1, a 2-D cross section of the flow placed orthogonal to the line of sight of the camera is illuminated by the laser beam. Fluorescent light

from the laser is then scattered by the particles present in the flow and collected by the high-speed camera. In order for these particles to accurately reflect the nature of the flow, it is imperative that they have specific properties including neutral buoyancy and small diameter which would guarantee accurate response to fluctuations in velocity. The diameter of the particles used in this study is on the order of 30 μm thereby greatly diminishing the possibility of a response-lag to velocity fluctuations. The light reflected by these particles is detected by the high speed camera which can record data successively via a frame rate as high as 1000 frames/sec. It should be mentioned that the frame rate and exposure time of the camera are subject to input as different configurations can be utilized for different purposes i.e. high exposure time and low frame rate for flow visualization.

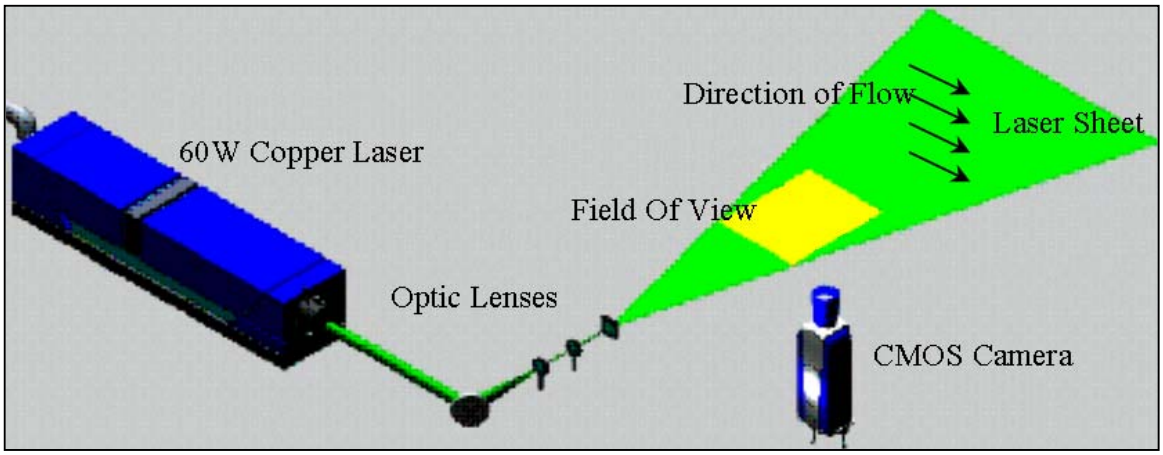

Figure 2.3.1 – Schematic representation of experimental setup including 60W pulsating Copper vapor laser, optic lenses, high speed CMOS Camera, and laser sheet (Pierrakos, 2002)

Images collected via the high speed camera are partitioned into square subdivisions such as 16x16 or 8x8 pixels. Each subdivision in then processed independently in order to obtain the measured displacements. Since the time step between each frame is known, the displacement can then be used to obtain velocity magnitude and direction. The vector density in the corresponding images is subject to a number of variables, among them the number of particles immersed in the flow and the number of interrogation windows. Cross-correlation in the Fourier domain is then applied to obtain particle displacement. The best way to actually describe this process is to superimpose two successive images and allow translation vertically and horizontally to produce the highest pattern of particle matching in both images. Corresponding displacement of the

pattern of particle images for the two frames is simply the distance of separation between the two windows. An algorithm already in place at our research facility allowed for the application of this technique thereby resulting in instantaneous maps of velocity distribution. Further processing using an in-house software was implemented to generate vorticity and turbulent kinetic energy distribution.

2.4 DPIV Experimental Setup

As illustrated in Figure 2.4.1, the experimental setup of the DPIV system allows for the generation of time-accurate velocity vectors along a plane orthogonal to the flow field. The current system employs a 60-Watt (although only a wattage of 30 W was produced at the time of data sampling) pulsating at a frequency of 10 kHz to deliver a plane of light to illuminate the area of interest. The behavior of the flow is manifested via the projection from the particles which act as flow tracers. A digital Complementary Metal Oxide Semiconductor (CMOS) imaging sensor sampling at 1000 frames/sec was integrated into the camera to capture the position of the particles at any given frame. For the purposes of this project, data was obtained for a duration of two seconds thereby resulting in 2000 independent frames. Due to prior knowledge of the vortex shedding frequency and the input frequency of the Coanda jet, such a time period was deemed to be an effective one for accurate representation of the flow. Cross-correlation, which was explained earlier, was then used between the particle image patterns of two consecutive frames. The tempo-spatial resolution of the DPIV system in question is adequate to understand the flow behavior of flow characteristics around a Coanda surface with circulation control. Currently, no previous results by other researchers applying DPIV to a circulation control study are known to the author.

The area of interest as shown in Figure 2.4.1 was approximately 80 mm by 80 mm (each dimension being approximately 53% of the chord length) at a camera resolution of 512 pixels by 512 pixels which translates to PIV magnification of approximately 158 microns per pixel. It is noteworthy to mention here that a significantly larger portion of the area around the Coanda surface was illuminated by the laser plane but due to the size of the area of interest, only a portion of the illuminated plane was zoomed into and analyzed. Since the location of the laser

source was underneath the airfoil, part of our image consists of incorrect data vectors resulting from the area that is covered by a shadow (see Figure 2.4.1). Though our software calculates vectors for this region, the results from this area are ignored. An additional item worth mentioning is that the pixel displacement in each direction was set to 8 when the data was processed thereby resulting in a vector spacing of 1264 μm (a product of the pixel displacement and the PIV magnification).

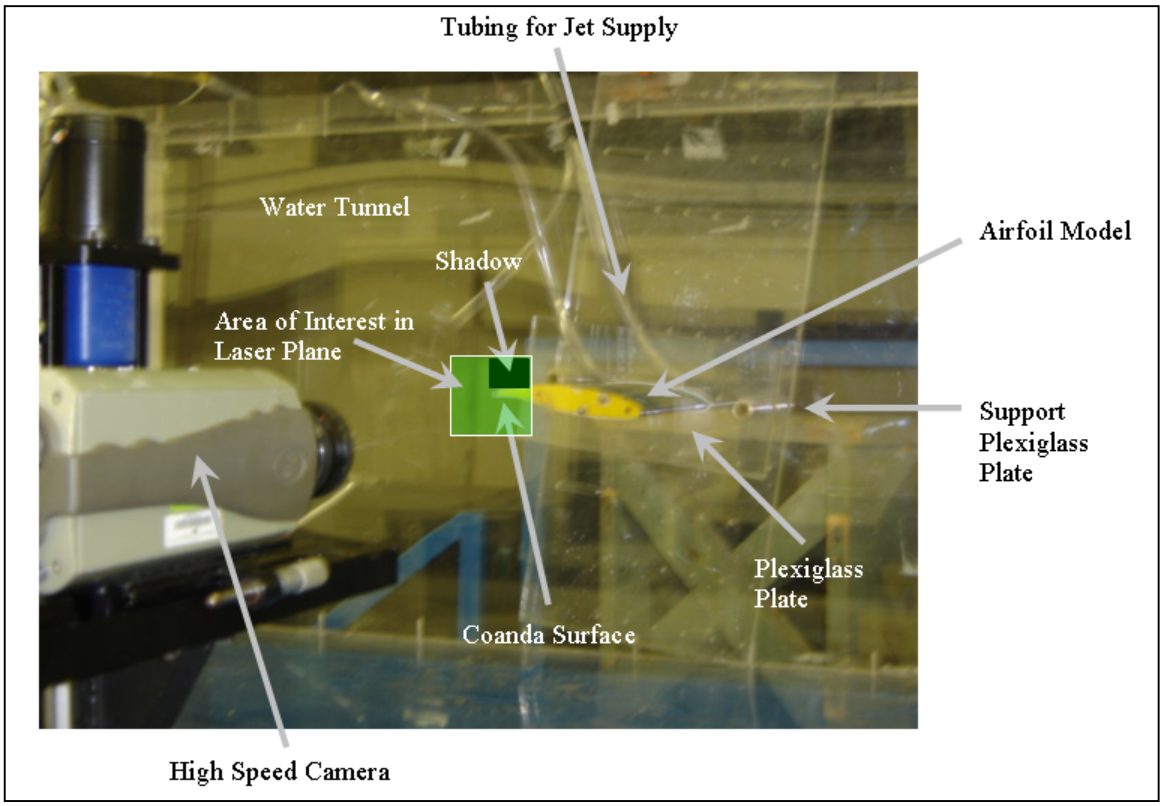

Figure 2.4.1 – Photograph of experimental setup with area of interest illuminated via pulsating laser

2.5 DPIV Hardware Component Details

Though the main components of the DPIV system were mentioned briefly in the preceding sections, the significance of the equipment entails a section that describes the role of each one as it applies to a DPIV setup. This section will provide a more detailed overview of the components including the pulsating fluorescent laser, the Phantom IV CMOS digital camera, and the optics.

2.5.1 60 W Pulsating Copper Vapor Laser

The 60 W high frequency (10 kHz) pulsating Copper Vapor laser has been the workhorse of the DPIV system at Virginia Tech for a number of years now. The laser, located in the ESM Fluid Mechanics Laboratory, has been the instrument of choice for a wide variety of applications including bio-fluid mechanics experiments and low speed aerodynamics, the latter of course being the subject of this particular paper. At the time of data collection, the laser was running only at a power of 30 W but this was deemed sufficient for the purposes of our experiment. It is also worth noting that the energy per pulse at optimal power is on the order of 5 mJ/burst. A schematic of the laser is shown in Figure 2.5.1.1.

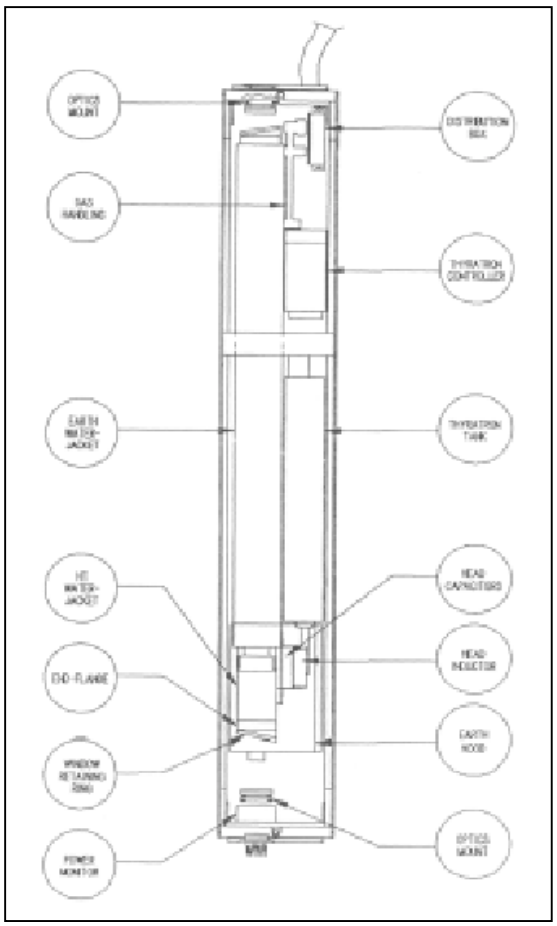

Figure 2.5.1.1 – Schematic of 60 W pulsating Copper vapor laser

2.5.2 Phantom IV High Speed CMOS Camera

The Phantom IV camera, manufactured by Vision Research Inc. capable of frame rates as high as 1000 frames per second (fps) for a 512x512 pixel resolution was used in conjunction with the high power laser and formed the backbone of the DPIV setup. Unlike other cameras used for flow visualization e.g. Charged Coupled Device (CCD) cameras, the camera in question has a higher signal-to-noise ratio thereby allowing for greater sensitivity. The frame rate used for our experiment was 1000 fps though the camera is capable of frame rates as high as 30,000 fps for reduced image format.

2.5.3 Optical Lenses

A combination of optical lenses was also used to obtain the necessary laser beam width of 2mm necessary for reducing the depth of field and distortion of out-of plane particles i.e. manipulating the laser plane to disregard any 3-D effects. The combination of the above components increased the interrogation and spatial resolution by a factor of four, while our maximum time resolution has increased by one order of magnitude, which is approximately one hundred times the corresponding time resolution delivered by commercial DPIV systems. Figure 2.3.1 shows an illustration of the optical arrangement used for the experimental setup.

2.6 General Aviation Circulation Control (GACC) Airfoil

The airfoil used in our study was a modified 2-D supercritical airfoil design constructed of stainless steel with a sectional lift coefficient of 3 and cruise drag coefficients consistent with traditional airfoils. The model, as shown in Figures 2.6.1 and 2.6.2, is based on a 17% supercritical airfoil section with blunt leading edges to minimize leading edge stall in addition to a dual-slot blowing effect on a small Coanda surface. The trailing edge consists of a circular Coanda surface with a radius-to-chord (r/c) ratio of 2%. The fluid for circulation control is introduced to the Coanda surface by means of thin slots (0.2 mm in height) tangential to the diameter of the Coanda surface. For our particular experiment, only the slot on suction side of the airfoil was used as this setting is beneficial for a high lift configuration. The chord length of

our airfoil was 6 inches with a span of 8 inches. The Coanda slots in the edge sections 0.65 in. from both the wing tip and wing root were taped off, hence only 6.7 in. of the slot length was actually used. In order to minimize 3-D flow effect at the tip, a plexiglass plate was attached at the airfoil tip. It is also noteworthy to mention that the zero-lift angle of attack for this type of model (without a Coanda jet in effect) is -6º as this was the angle of attack used for our experiment. A more accurate visual description of the trailing edge Coanda surface is illustrated in Figure 2.6.3.

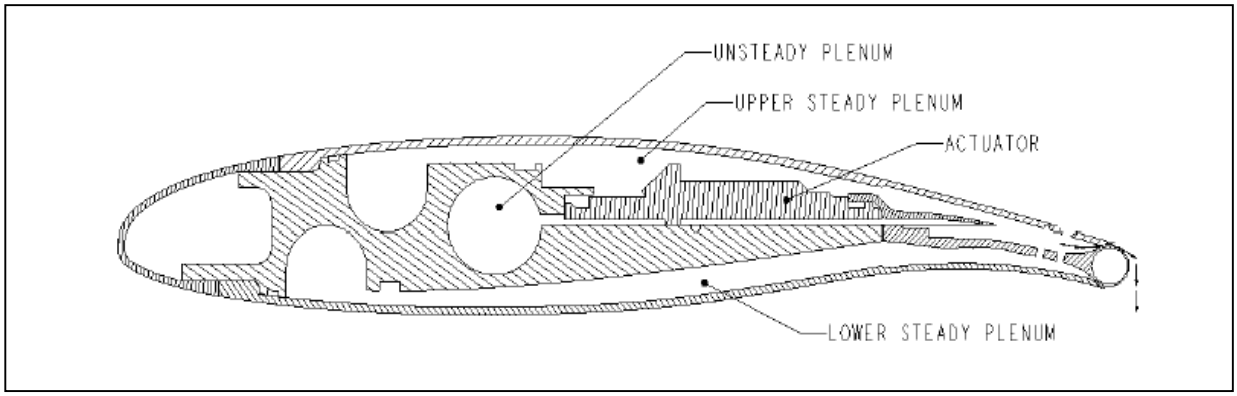

Figure 2.6.1 – Schematic of General Aviation Circulation Control (GACC) airfoil (Cagle, 2002)

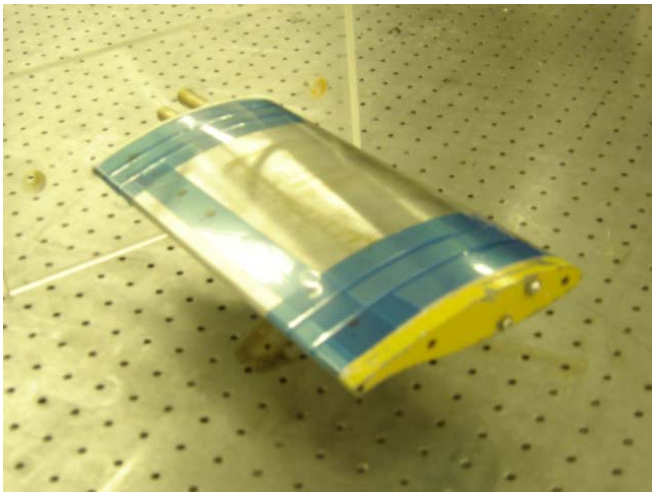

Figure 2.6.2 – Image of water tunnel based General Aviation Circulation Control (GACC) airfoil model

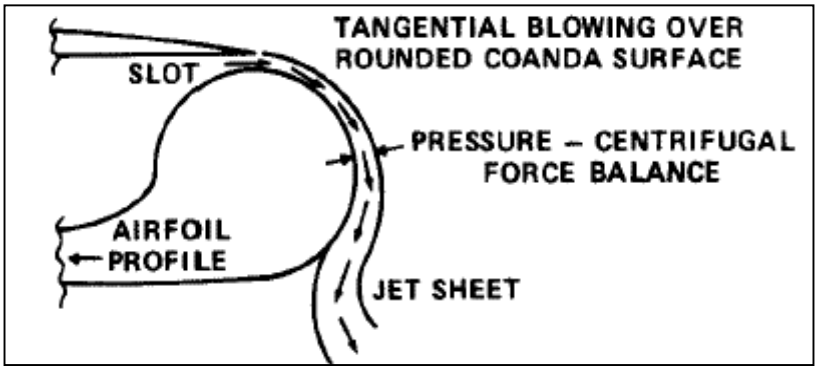

Figure 2.6.3 – Schematic of Trailing Edge Coanda Effect for GACC Airfoil

2.7 Data Acquisition Test Matrix

A total of 11 test cases were used for data sampling in our experiment as illustrated in Table 2.7.2. The first case involved no Coanda jet whereas there were five cases each for steady flow and pulsed flow at a frequency of 1 Hz. Due to limitations on our hardware, pulsed frequencies above 1 Hz could not be achieved. In all cases, a freestream velocity of 15 cms-^{1} was used. Note that this corresponds to a value equivalent to one chord per second. The equivalent frequency, denoted as f^{+}, is the product of the actual frequency and the ratio of the characteristic length over the mean freestream (see Table 2.7.1). Note that this is somewhat analogous to the Strouhal Number where the airfoil thickness is used as the characteristic length. Since we have chosen our freestream to correspond to one chord length per second, numerically our values for actual frequency and reduced frequency will be equivalent. The second column in our test matrix has the volumetric flow rate which was read by a flow meter connected to the tubing used to provide the fluid to the Coanda jet. This flow rate is then used to derive the maximum jet velocity. Note that this velocity corresponds to the value at the jet exit when the jet exits the slot. Due to mixing with the freestream that takes place aft of the Coanda jet slot, there is a rapid increase in spread size of the jet which corresponds to a rapid velocity drop. Data collected even a fraction of a chord length downstream of the Coanda surface will yield velocity measurements that are lower than those at the jet exit by an order of magnitude or more. The last column gives us the value for momentum coefficient which is essentially the ratio of the force contributed by the jet and that contributed by the freestream. These are defined in Table 2.7.1.

Reduced Frequency	Strouhal Number	Momentum Coefficient
$f^+ = \frac{f \times \bar{c}}{U_o}$	$St = \frac{f \times t}{U_o}$	$C_\mu = \frac{Coanda\ Jet\ Thrust}{Freestream\ Force} = \frac{\dot{m} \times U_{jet}}{q \times S \times \bar{c}}$

Table 2.7.1 – Definitions of Reduced Frequency, Strouhal Number, and Momentum Coefficient

	Freestream Velocity Uo (m/s)	**Vol. Flow Rate Q (L/min)**	**Jet Velocity Uj (m/s)**	**Mom. Coefficient Cμ**
Steady (0 Hz)	0.15	0.00	0.00	0.00
	0.15	2.56	1.25	0.15
	0.15	5.07	2.48	0.60
	0.15	7.59	3.72	1.35
	0.15	10.10	4.95	2.39
	0.15	10.70	5.24	2.68
Pulsed (1Hz)	0.15	0.82	0.40	0.02
	0.15	2.11	1.03	0.10
	0.15	3.17	1.55	0.24
	0.15	4.21	2.06	0.42
	0.15	5.06	2.48	0.60

Table 2.7.2 – Data Acquisition Test Matrix including flow rates, maximum jet velocities, and momentum coefficients

CHAPTER 3

3 EXPERIMENTAL RESULTS

3.1 Time Averaged Vorticity Distribution

During our study, five cases were taken for each of the actuation conditions, pulsed and steady in addition to a baseline case with no flow control. Due to the variety of data available, our cases can be sorted by the actuation Strouhal Number, or the type of data analysis (time-averaged or time-resolved). The initial presentation of our results will be based on the latter although it will be further analyzed based on the Strouhal Number.

3.1.1 Time Averaged Vorticity Distribution (Steady)

The first five cases to be presented employ steady blowing with no driving frequency. The baseline case, presented here as the first picture, is for a momentum coefficient of zero (no blowing). The other five cases are shown with an increasing momentum coefficient, and each one is labeled.

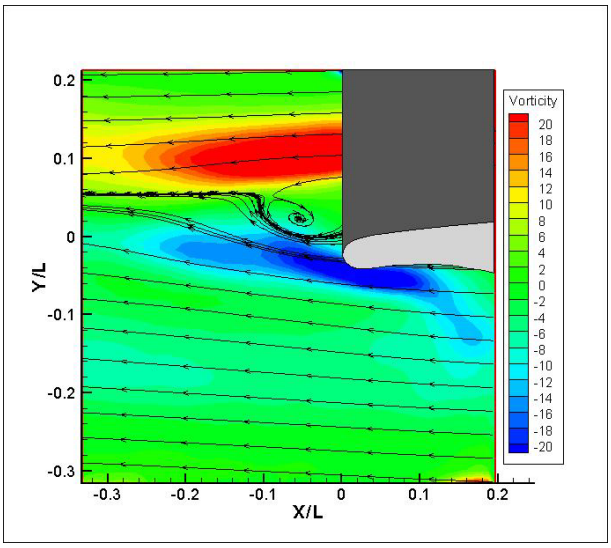

(a: $C_\mu = 0.00$)

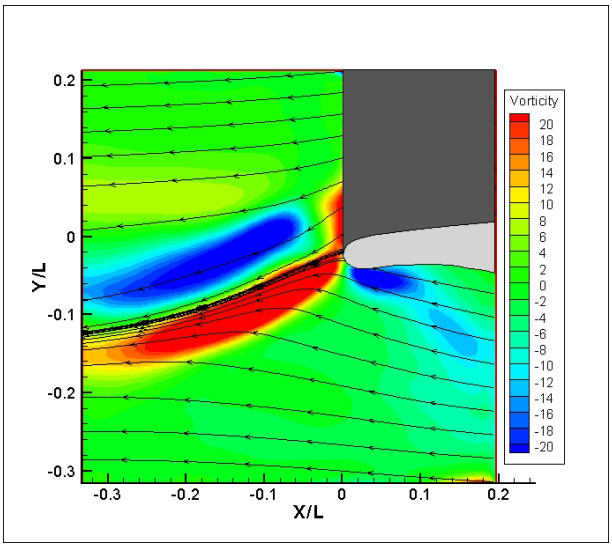

(b: $C_\mu = 0.15$)

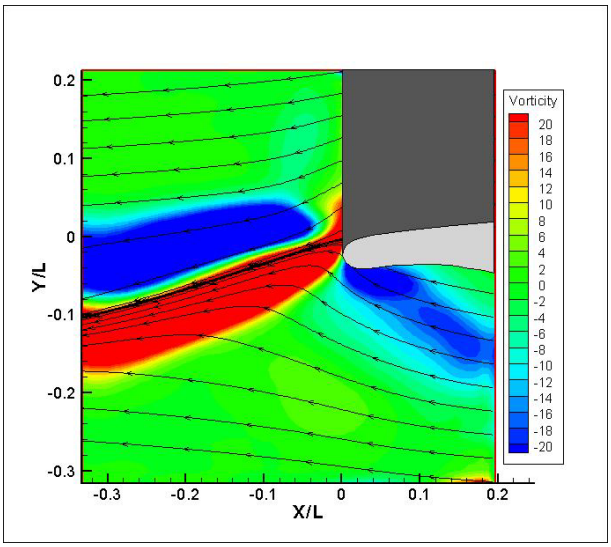

(c: $C_\mu = 0.60$)

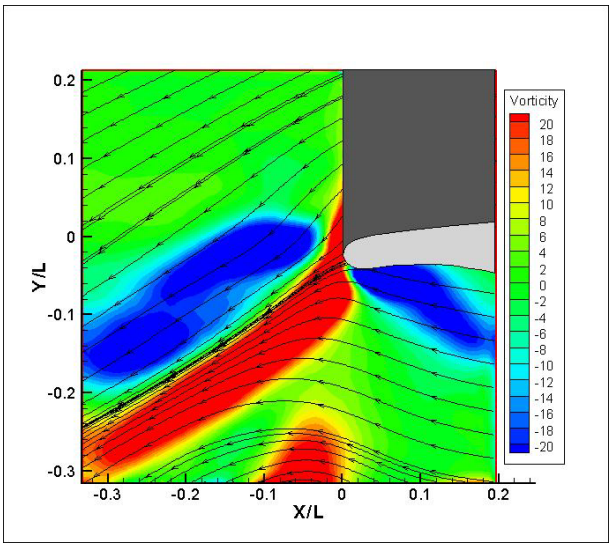

(d: $C_\mu = 1.35$)

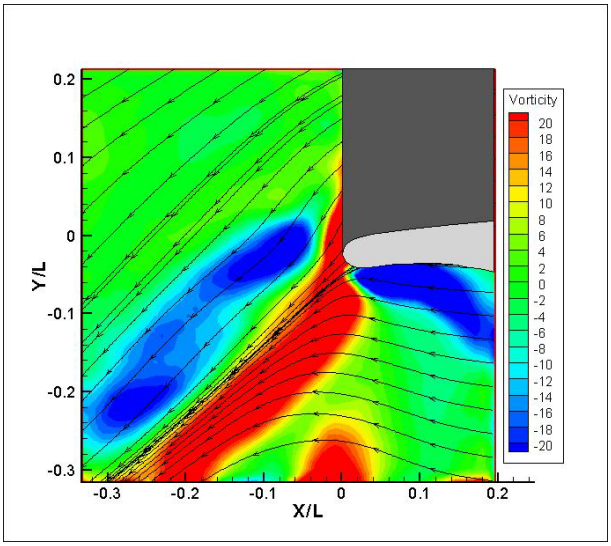

(e: $C_\mu = 2.39$)

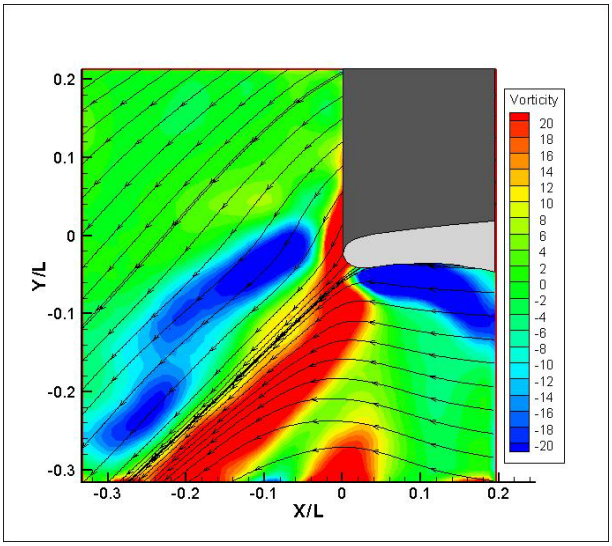

(f: $C_\mu = 2.68$)

Figure 3.1.1.1 – Vorticity contours of time averaged results for various steady momentum coefficients

Recall that our airfoil was placed at a zero lift angle of attack. As can be seen, the flow is clearly separated over the airfoil and we can observe the vortices shed on the suction and pressure side of the airfoil. This is in agreement with out intuition that the thickness of the airfoil combined with the high camber and the rounded trailing edge will all contribute to vortex shedding. Note that in all of the other cases, this is not the case though the angle of attack

remains unchanged. That is because the momentum influx resulting from the Coanda jet creates a virtual trailing edge and creates a back stagnation point that shifts upstream as the Cμ is increasing. This implies that the circulation thus the lift over the airfoil should increase.

Also note that in the case (a), the vorticity sign is the opposite of that in cases (b) through (f). In case (a), the regions of positive and negative vorticity are centered at (X/L, Y/L) = (-0.05, 0.10) and (-0.04, -0.04). The vorticity signs are consistent with what one would observe in a circular cylinder immersed in a flow i.e. no lift acting on the body. The vortices that can be seen in this image are resultant of separated flow on either surface of the airfoil. As the jet is imparted on the flow however, there is a clear reversal of the vorticity signs as illustrated in figures (b) through (f). More specifically, the regions of positive and negative vorticity in case (b) relocate to (X/L, Y/L) = (-0.15, -0.05) and (-0.15, -0.12) respectively. As will be explained in the next chapter, the Coanda jet acts to force the flow from the suction side towards the trailing edge and in doing so, pulls in the streamlines such that we can see the flow reattach to the surface. The change in the flow physics that directly contribute to the change in signs of the vorticity are rooted in the shape of the velocity profile downstream of the airfoil. These changes and the vorticity signs associated with them will be discussed in more depth in the Chapter 4.

Figures (b) through (f) also reveal a clear change in the flow deflection angle as the momentum coefficient is increased. As would be expected, a higher value of C_μ results in greater deflection in the streamlines. Note that this is analogous to the streamline behavior for a control surface such as a flap. In addition to the change in angle, focus on the increased circulation that result from the momentum contribution. In figure (b), we observe that the streamline intersects the airfoil at the location of the jet i.e. X/L = 0. In figure (f) however, note that the point of intersection is clearly located on the pressure side at a location of X/L = 0.03. It is evident that the higher value of momentum coefficient acts to force the rear stagnation point upstream as we had expected. Recall that a greater translation of this location has a direct effect on the lift acting on the body. We can see that in each of the intermediate figures, i.e. (c) through (e), there is increase in circulation due to the jet impact which in turn amplifies the net lift acting on the body.

In all of the frames, note an area of negative vorticity on the pressure side. This will be explained in more detail when the time-resolved images are discussed but it is clear that this contribution is made from flow upstream. Although we did not record data upstream we hypothesize that shed vortices resulting from leading edge flow separation are responsible for the negative vorticity observed.

3.1.2 Time Averaged Vorticity Distribution (Pulsed)

Again, we will present the baseline case i.e. no actuator frequency, first. The other five cases are shown with an increasing momentum coefficient, and each one is labeled. The latter five cases are all at a driver frequency of 1 Hz which translates to a reduced frequency (f^+) of 1 and a Strouhal Number (St) of 0.17.

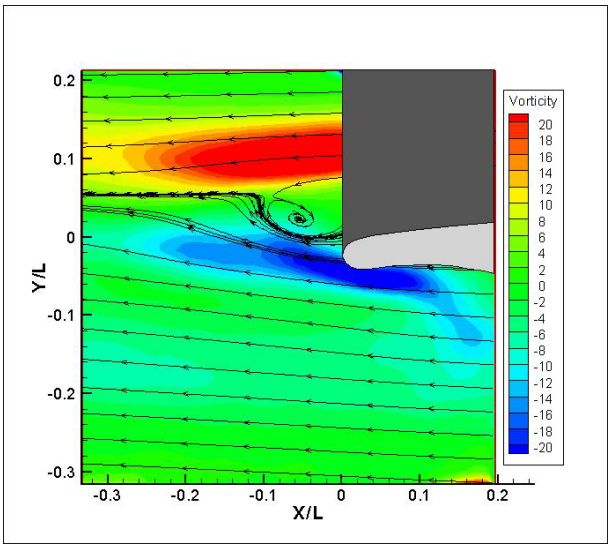

(a: $C_\mu = 0.00$)

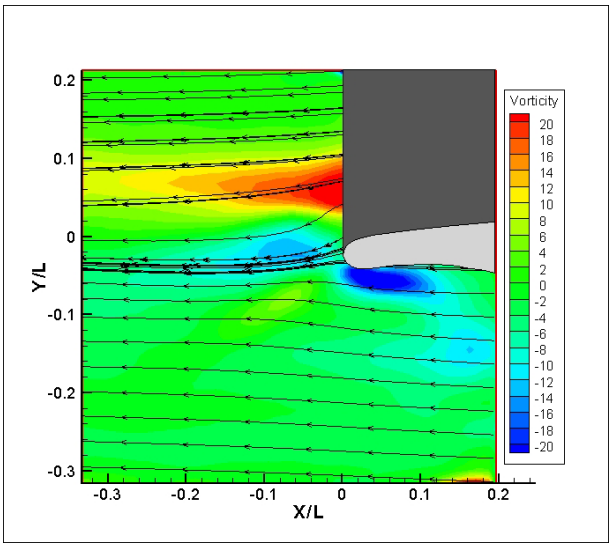

(b: $C_\mu = 0.02$)

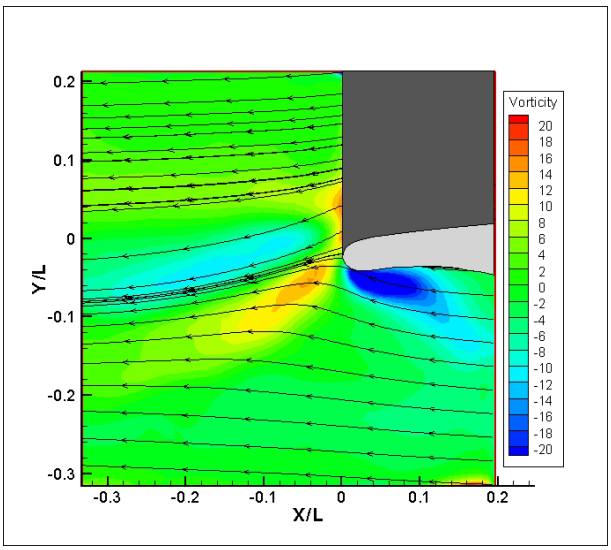

(c: $C_\mu = 0.10$)

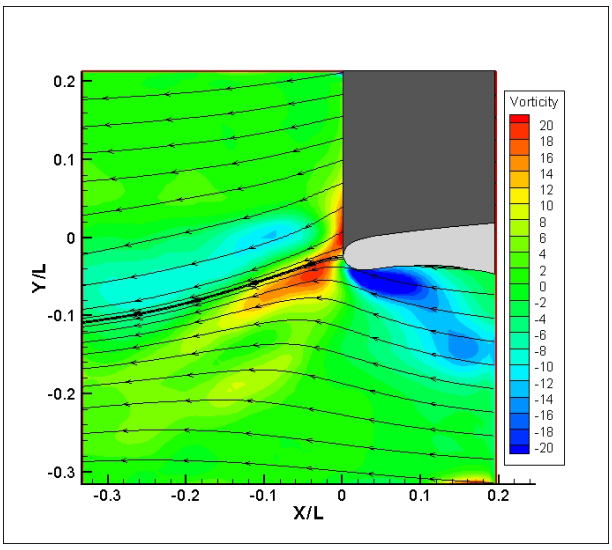

(d: $C_\mu = 0.24$)

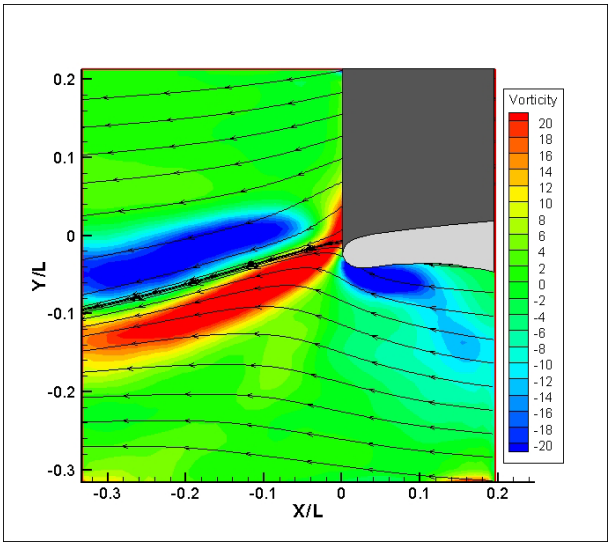

(e: $C_\mu = 0.42$)

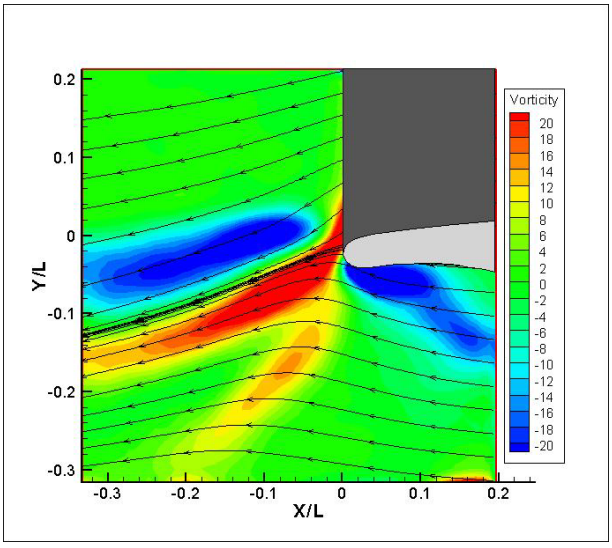

(f: $C_\mu = 0.60$)

Figure 3.1.2.1 – Vorticity contours of time averaged results for various pulsed momentum coefficients

We can now repeat our procedure for the results of flow using unsteady forcing. Before we move further, recall that we are still analyzing the results in a time-averaged sense. Therefore, our image is effectively the mean of two complete cycles in the two second period for which we sampled data. Hence, what we are viewing are the averaged results between the peak and trough of the cycles.

Observe that in Figure 3.1.2.1 (a) and (b), the flow is separated. We would expect this to be the case with the former but because our momentum coefficient is very low ($C_\mu = 0.02$) in the second case as well, not a significant enough force is imparted to maintain an attached flow. Note however, that this value corresponds to the peak of the cycle whereas our image is reflective of the time average. Thus, there will be some locations in the cycle i.e. near the peak, where we will have attached flow. Figure (c) clearly shows the reversal in the vorticity sign that was discussed in the previous section. The area in the light blue shade centered at X/L = -0.15 has negative vorticity. In the subsequent frames, we can see that the strength of this area increases as the momentum coefficient is amplified.

Also note that there are two areas of positive vorticity in frame (f). Because our frame takes into account both the peak of the cycle (which in this case corresponds to a C_μ of 0.60) as well as the location where there is no jet i.e. trough, we see areas of vorticity corresponding to both. The location centered at Y/L = -0.17 is resulting from the highest momentum coefficient. We can also conclude that our streamlines will be temporally active between these two regions of positive vorticity.

3.1.3 Time Averaged Vorticity Distribution for $C_\mu = 0.60$

In order to further examine the difference in flow behavior between the steady and pulsed cases, two samples with the same momentum coefficient were isolated for further study. Shown here are the results for a C_μ of 0.60 for both unpulsed and pulsed cases.

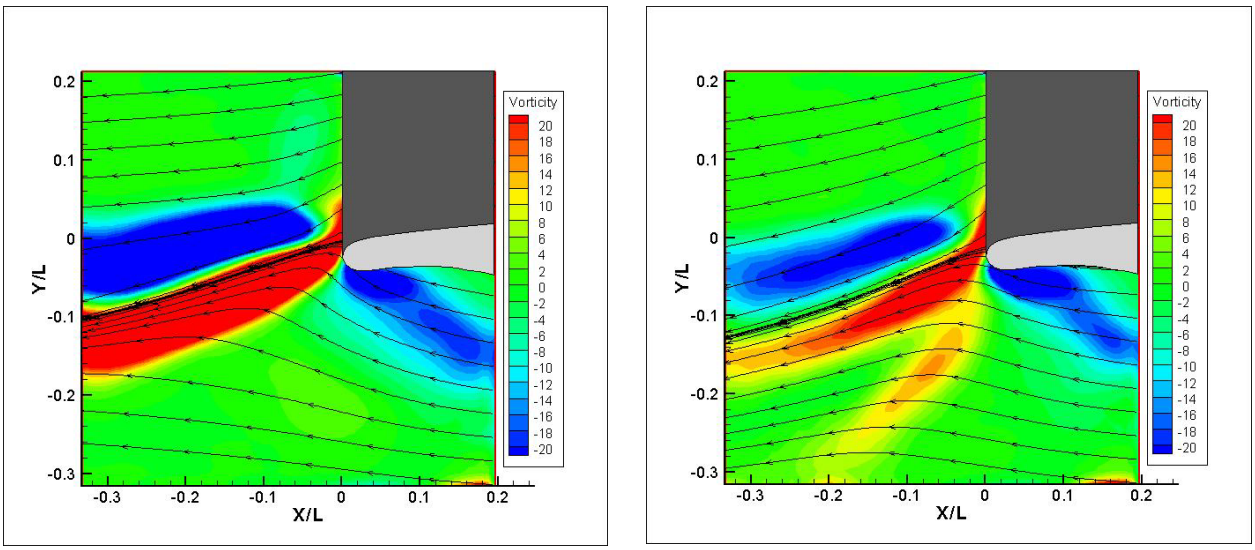

Figure 3.1.3.1 – Vorticity contours of time averaged results for steady (left) and pulsed (right) cases for a momentum coefficient of 0.60

We can continue our discussion of the time-averaged case of a temporally variant flow by directly comparing the results of steady and unsteady flow at a fixed momentum coefficient of 0.60. Note that although in the steady case, the jet is not cyclic, there will be some variations present in the angle of deflection resulting from the RMS of the jet velocity. On the frame on the right in Figure 3.1.3.1, we can see the impact that the cyclic jet has on the time-averaged strength of vorticity. Specifically, we see two independent regions of positive vorticity centered at (X/L, Y/L) = (-0.06, -0.08) and (-0.06, -0.17) respectively. The latter location corresponds to the peak of the cycle (highest momentum coefficient) while the former is resultant from the trough of the cycle. Also note that the average strength of each of the positive areas is lower than that corresponding to the steady case as can be seen from the lighter shade of color.

A point of interest that we observe when viewing our two frames simultaneously is that the flow is not deflected by the same amount. It is clear from Figure 3.1.3.1 that the deflection is somewhat greater in the second case. In the steady case, we can see an intersection at Y/L = 0.1 whereas in the pulsed case, the intersection is at Y/L = -0.15. Recall from our analogy with a control surface such as a flap, that this corresponds to a greater lift force acting on the wing. Bearing in mind that a duty cycle of 50% was used, what we are effectively stating is that we can improve the lift coefficient at half the energy expenditure.

3.2 Velocity Spectra

Though the vorticity plots cases yield considerable information on the behavior of flow at the trailing edge, what they do not do is provide us with a quantitative way of measuring the shedding frequency of the vortices over our airfoil or any other inherent unsteadiness. In order to fill this gap, a program was developed in MATLAB® to calculate this information from the measured velocities. The algorithm works by inputting the time records of the velocity vectors. The fluctuation in the velocity can then be used to measure the frequency. The plot presents the energy magnitude for a given vertical location (y-axis) as a function of the Strouhal Number. Note that both axes are dimensionless, for y-location we non-dimensionalize using the characteristic length and the x-axis has a St value based on the thickness of the airfoil (see Figure 2.7.1). To generate the plots, velocity fluctuation at equally spaced locations downstream of the Coanda jet were used (see Figure 3.2.1.1). Each plane is roughly 4% of the chord length apart which translates to a physical distance of roughly 0.6 cm.

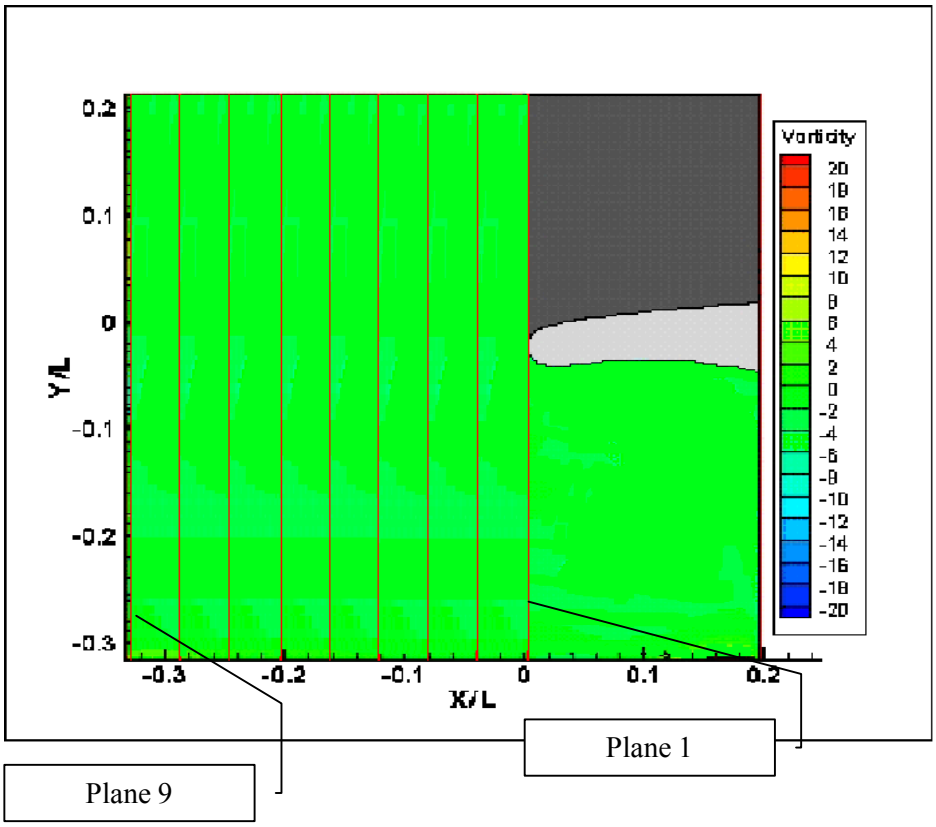

Figure 3.2.1.1 – Schematic of Planar Locations corresponding to Velocity Spectra

3.2.1 Velocity Spectra - Steady

Figure 3.2.1.2 shows our velocity spectra for steady blowing flow control. Each frame corresponds to the six cases that were used for momentum coefficients.

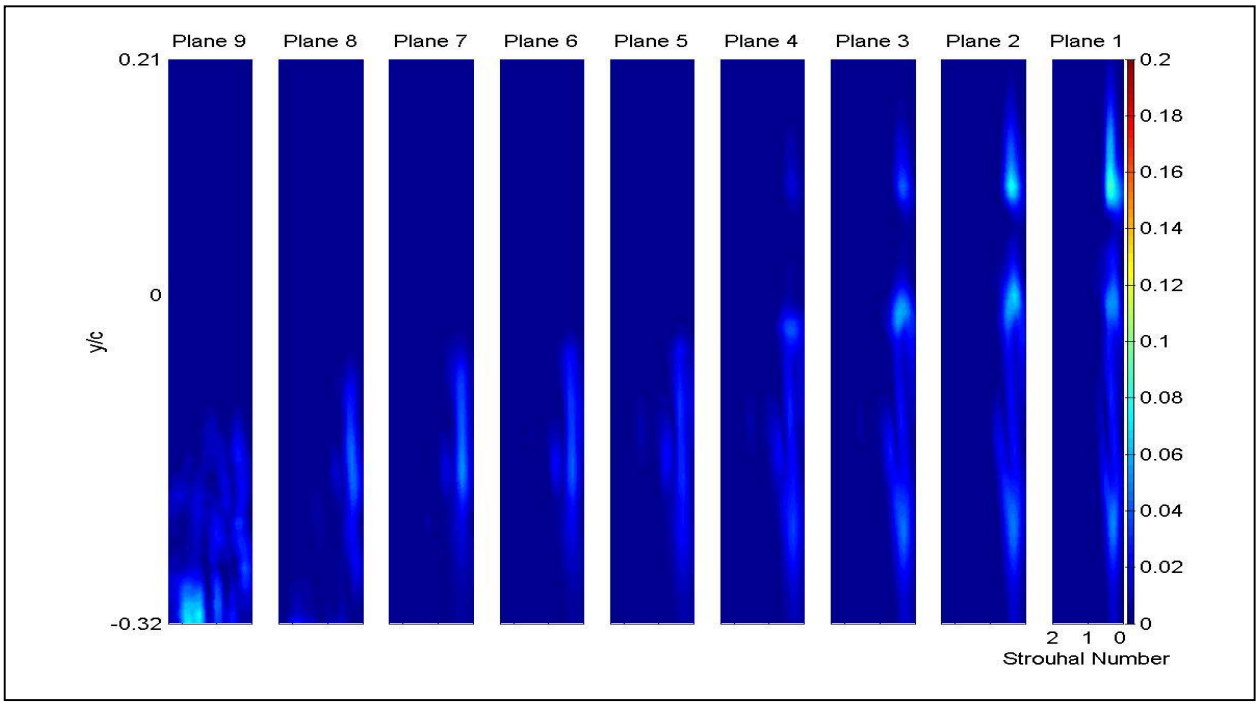

$C_\mu = 0.00$

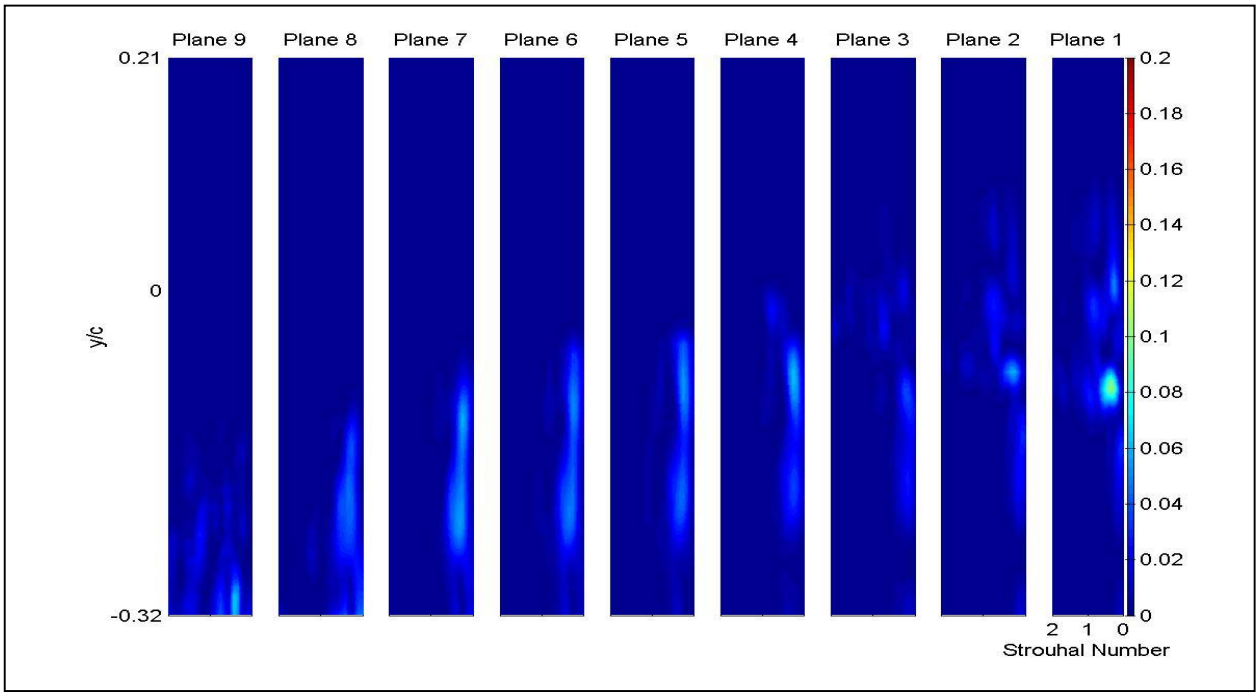

$C_\mu = 0.15$

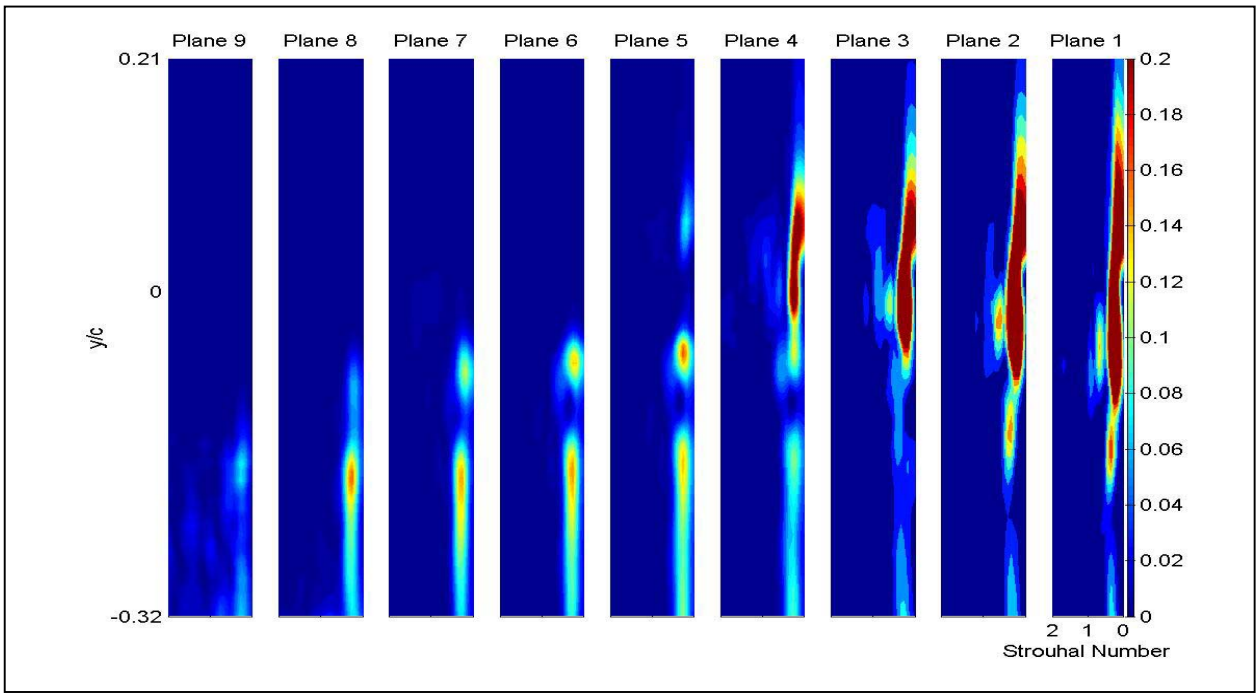

$C_\mu = 0.60$

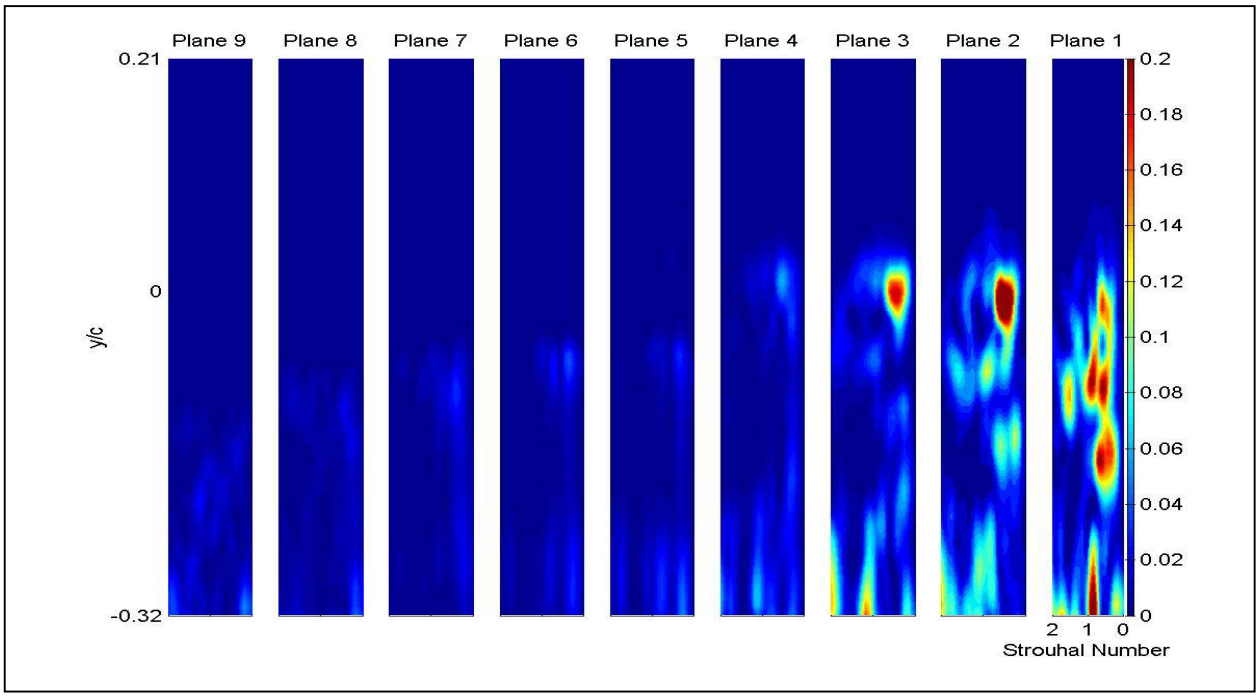

$C_\mu = 1.35$

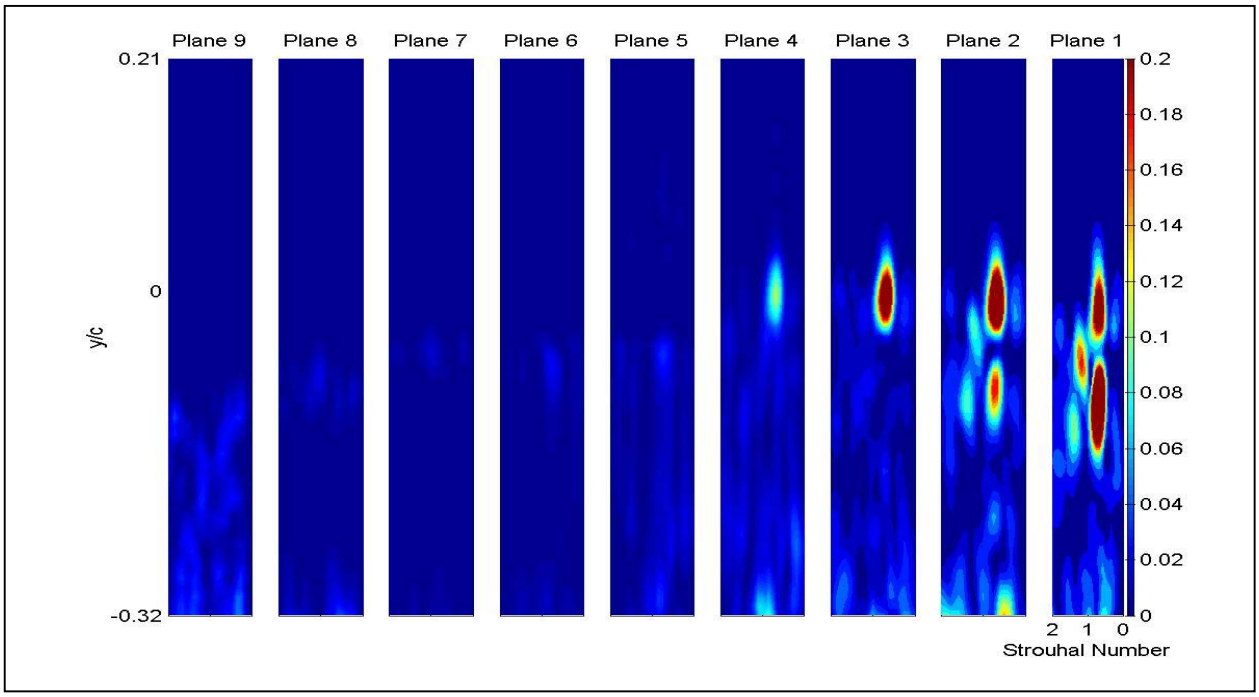

$C_\mu = 2.39$

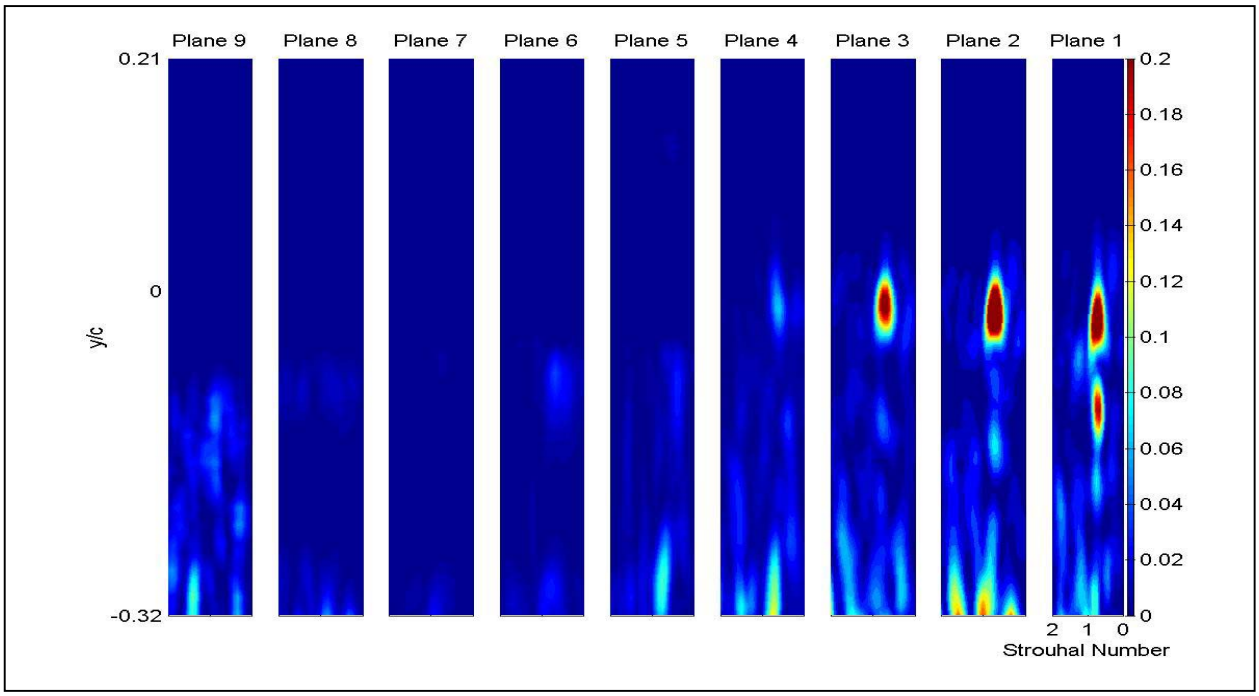

$C_\mu = 2.68$

Figure 3.2.1.2 – Velocity spectra of time averaged results for various steady momentum coefficients

The frames shown in Figure 3.2.1.2 clearly indicate an intensification of velocity fluctuation strength for greater momentum coefficients. Note, however, that the dimensionless frequency in frames (a) through (c) is consistent at a St ≈ 0.3. At higher momentum coefficient values, however, the primary Strouhal Number is significantly higher i.e. St ≈ 0.9. Also note that there is a tendency for weaker vortices to form on the suction side as can be seen in all of the frames and they dissipate at a downstream location closer to the Coanda surface.

3.2.2 Velocity Spectra-Pulsed

We repeat the results here for the pulsed case. The same program was implemented to generate these plots. Due to the nature of the Coanda jet however, one can notice significant differences in the behavior of vortex shedding. These will be discussed in the next chapter.

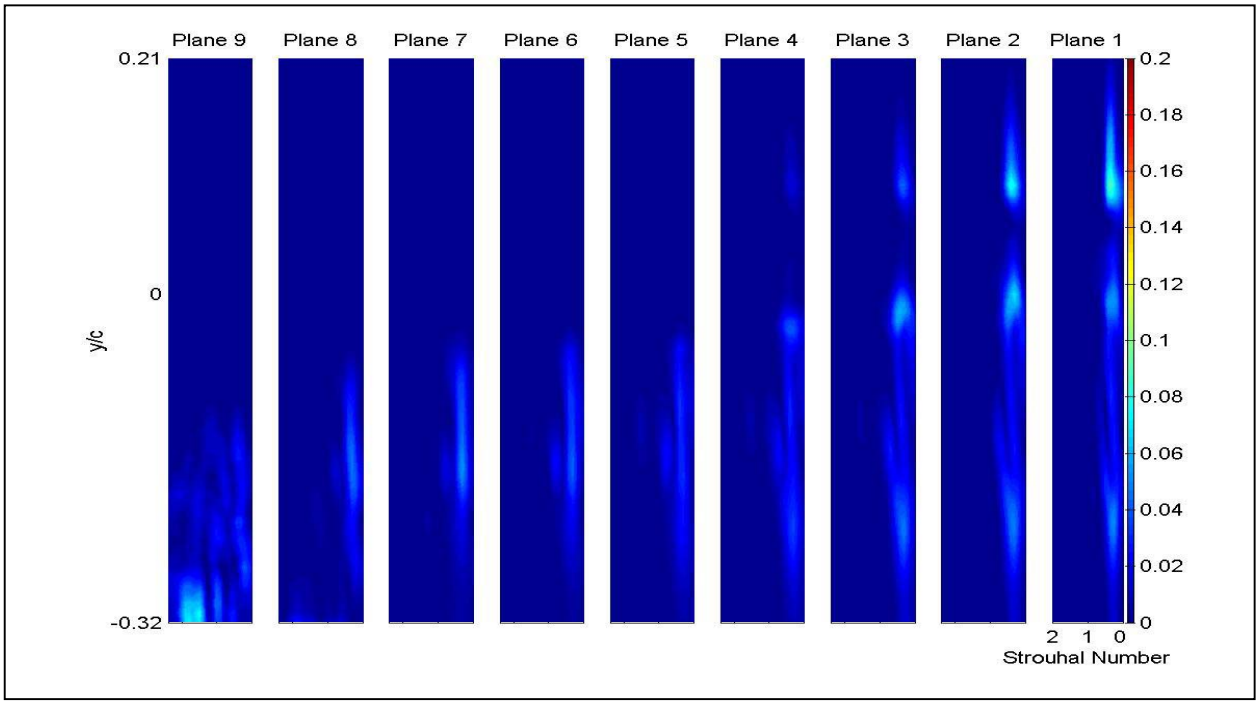

$C_\mu = 0.00$

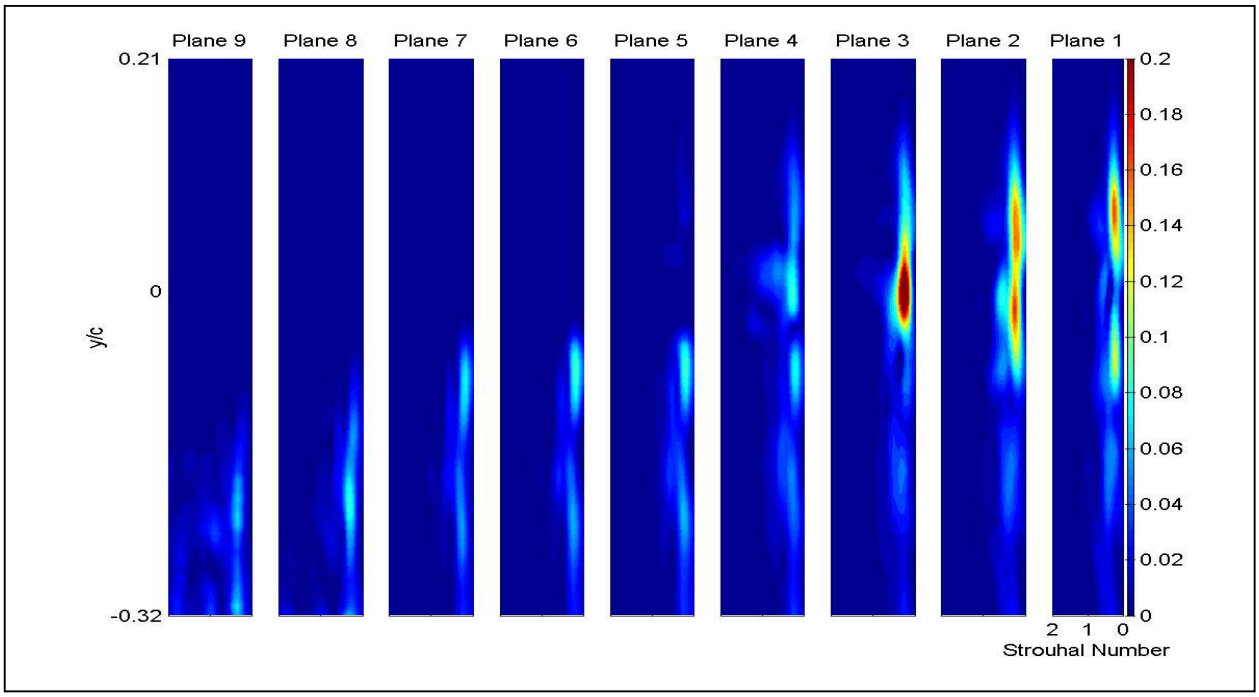

$C_\mu = 0.02$

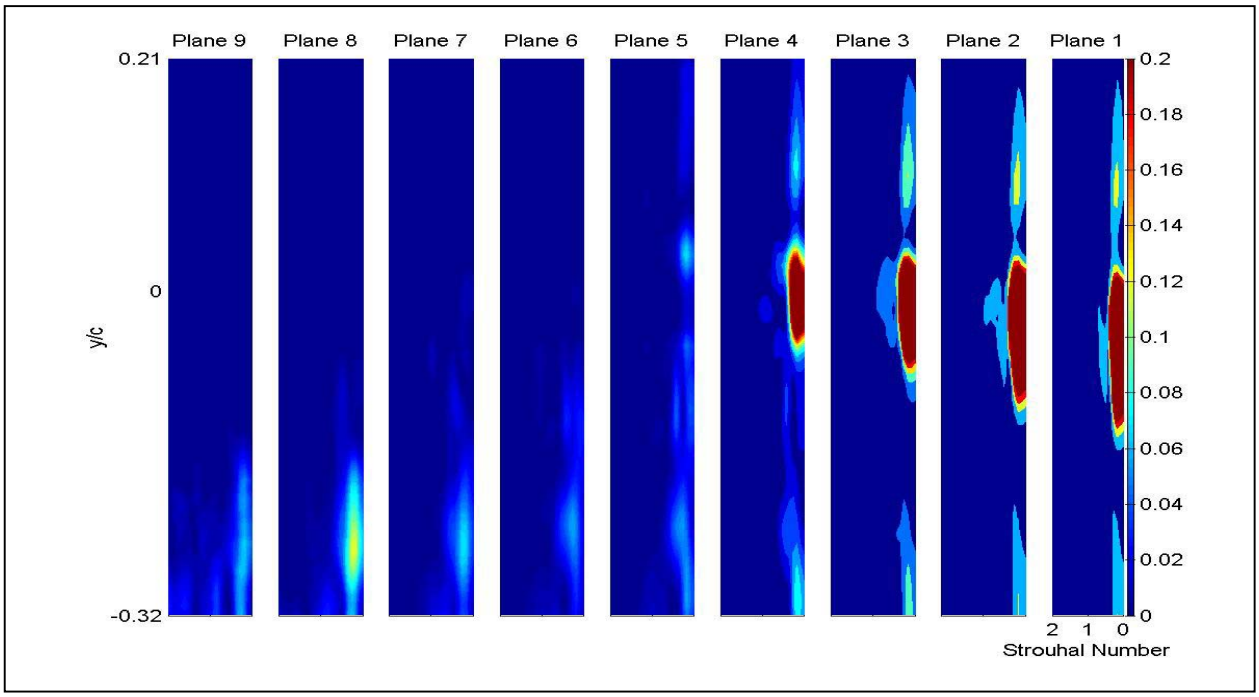

$C_\mu = 0.10$

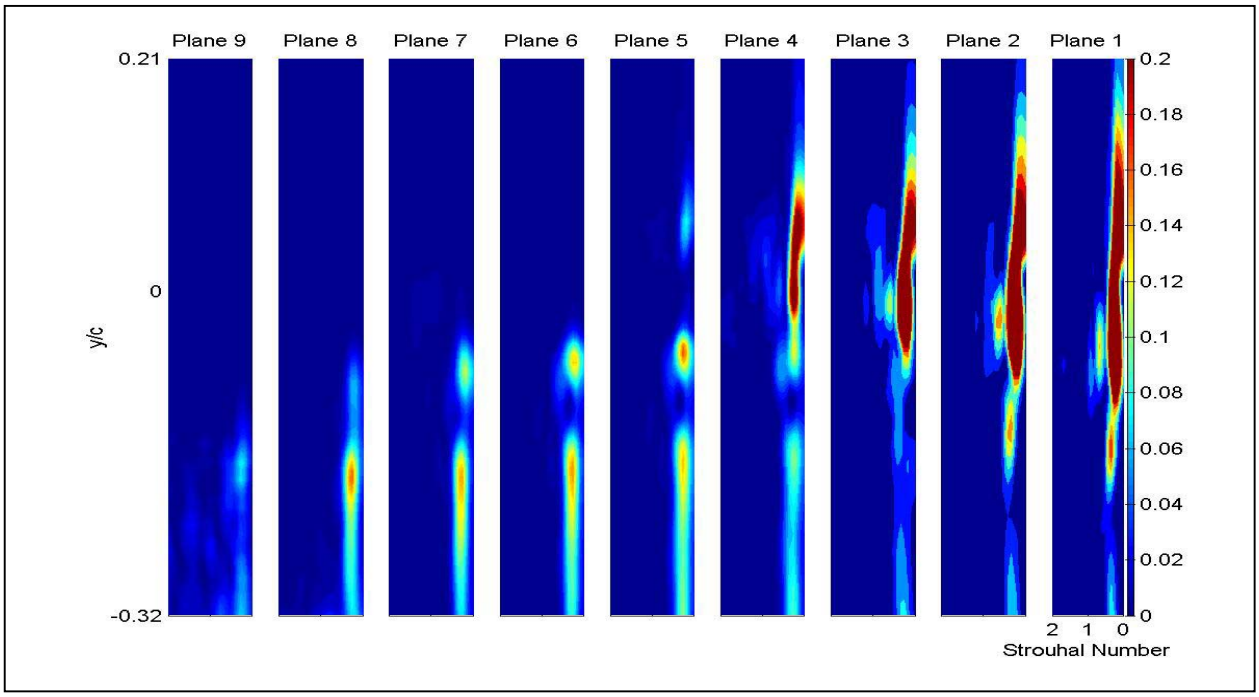

$C_\mu = 0.24$

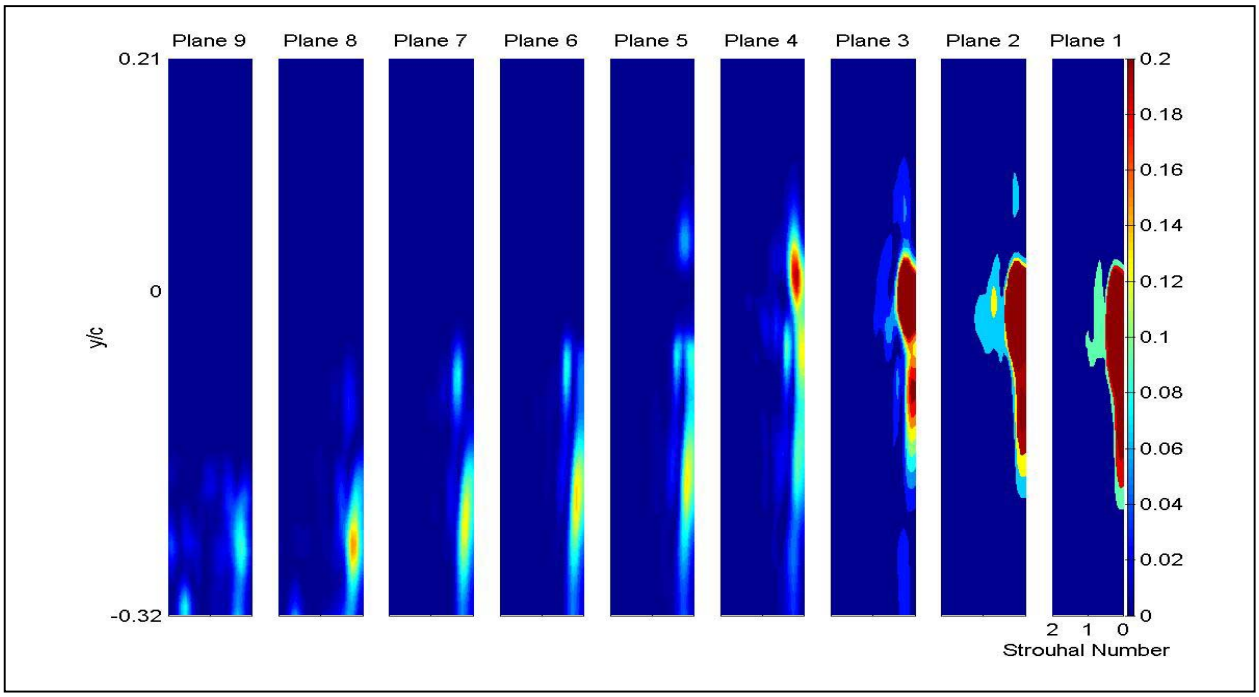

$C_\mu = 0.42$

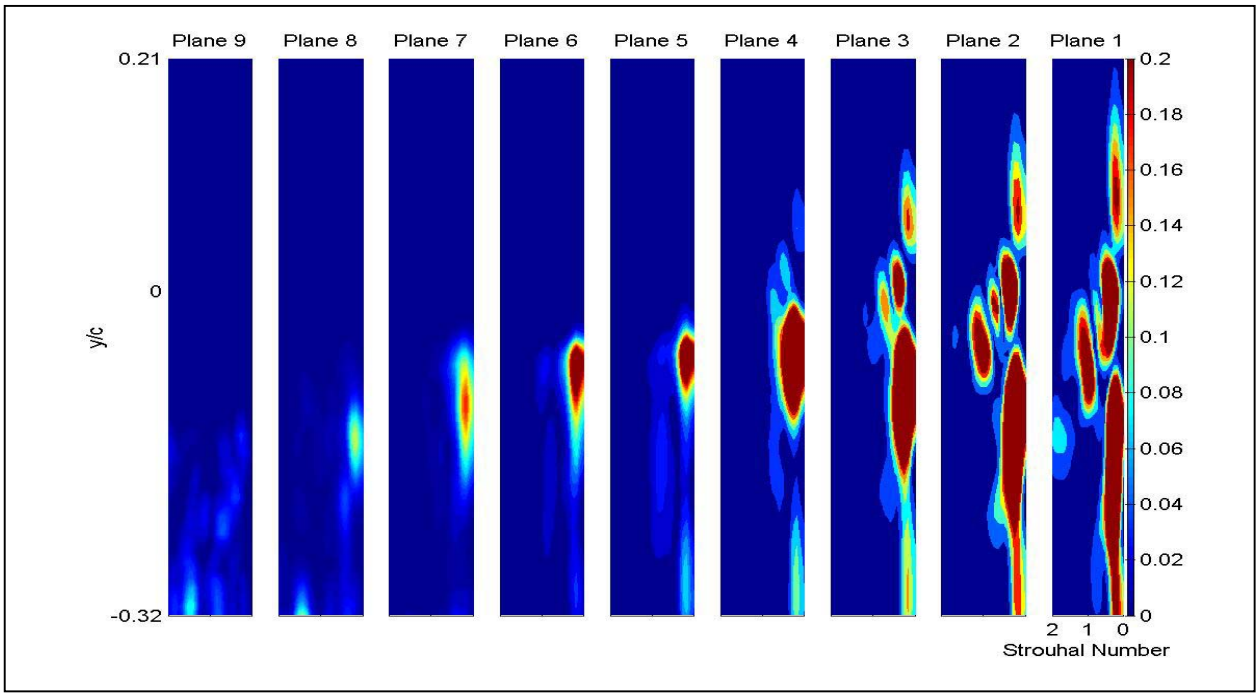

$C_\mu = 0.60$

Figure 3.2.2.1 – Velocity spectra of time averaged results for various pulsed momentum coefficients

The results of our procedure for the time-variant case indicate slightly different results. One of the first things that we observe is that by and large, the strength of the vortices is significantly greater in this case than for the steady blowing case. Also note that for cases (a) through (e) in Figure 3.2.2.1, we see the same value for Strouhal Number that was illustrated in the previous section. However, upon closer inspection of frame (f), we see that for a higher value of C_μ, we have two locations of significant velocity fluctuation. Note also that the weaker vortices have a much higher Strouhal Number associated with them ($St \approx 1$).

3.2.3 Time Averaged Velocity Spectra for $C_\mu = 0.60$

In order to analyze the difference in the flow unsteadiness between the steady and pulsed case, we will view the two cases corresponding to a C_μ of 0.60.

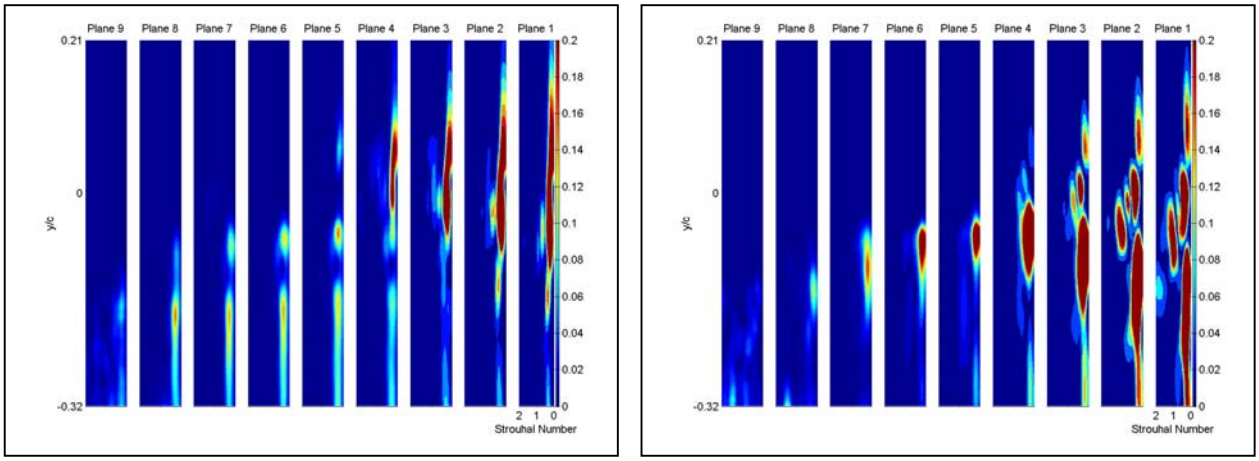

Figure 3.2.3.1 – Vortex shedding frequency plots of time averaged results for steady (left) and pulsed (right) cases for a momentum coefficient of 0.60

By comparing the spectra of our case of $C_\mu = 0.60$, we see two primary differences. Firstly, in the case of a pulsed jet, there is the presence of a second weaker vortex that has a Strouhal Number that is three times as great ($St \approx 0.9$). Both of the vortices in the second case take longer to dissipate. Also observe that in both cases, the vortices at a location above $y/c = 0$ terminate abruptly after Plane 4.

3.3 Time Resolved Vorticity Distribution

A unique contribution if the current work stems from the ability of the Time Resolved DPIV system used to capture over 2000 frames of data in a two second period thereby giving us an opportunity to analyze the flow behavior in two complete cycles. Though this type of data is better analyzed using animations, where each instant for the flow is presented in sequential order, within this text we have to resort to a frame-by-frame demonstration. This section will contain the images resulting from the time resolved output. The first frame of each sequence is reference

to t = 0 that corresponds to the trough of the cycle. Each succeeding frame is labeled by the time at which it was taken. Note that for the steady blowing cases, the time is referenced to an arbitrary value since there is no physical event that can be used to time stamp the data. The main objective here is to analyze the behavior of vorticity at the trailing edge as the forcing jet is applied. Note that the maximum instantaneous momentum coefficient is used for the value of C_μ. During the cycle the value of C_μ will fluctuate between this value and zero.

3.3.1 Time Resolved Vorticity Distribution (Steady @ C_μ = 0.15)

The first case to be presented here is the lowest non-zero momentum coefficient value (C_μ) of 0.15 for the case of a reduced frequency, f^+, is 0. All six frames shown in Figure 3.3.1.1 illustrate clear consistency among the cases used (regardless of the time the frame corresponds to). That being said, the deflection angles of the streamlines vary from case to case. The frame corresponding to t = 0.36 sec shows an intersection point at Y/L = -0.11 whereas in the frame corresponding to t = 0.54 sec, the streamline intersects Y/L at -0.17. We can attribute this to the velocity fluctuation resulting from the jet.

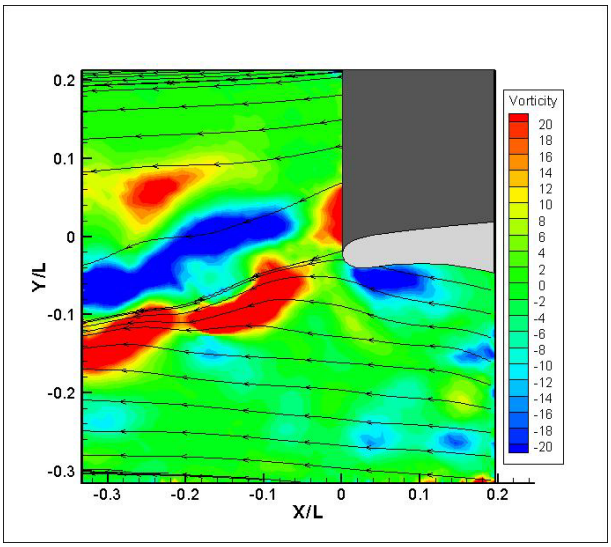

t = 0.00 sec

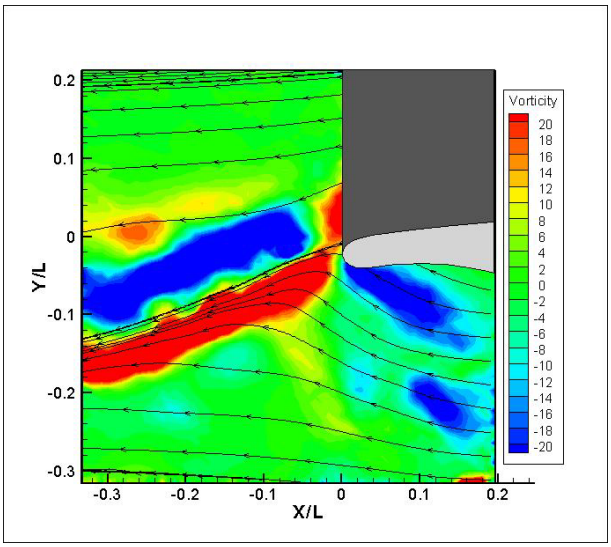

t = 0.18 sec

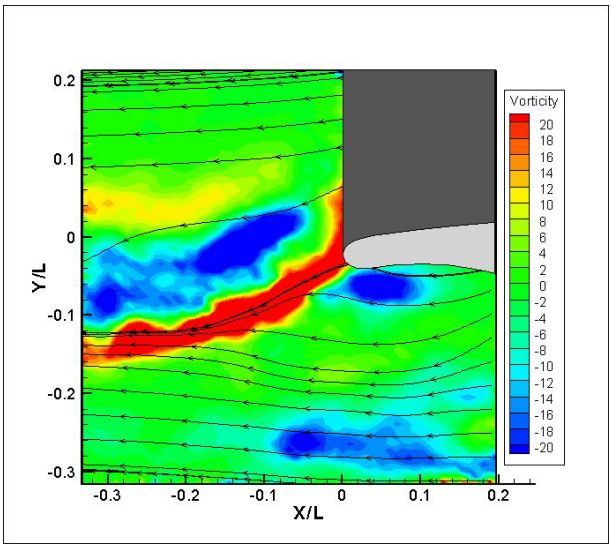

t = 0.36 sec

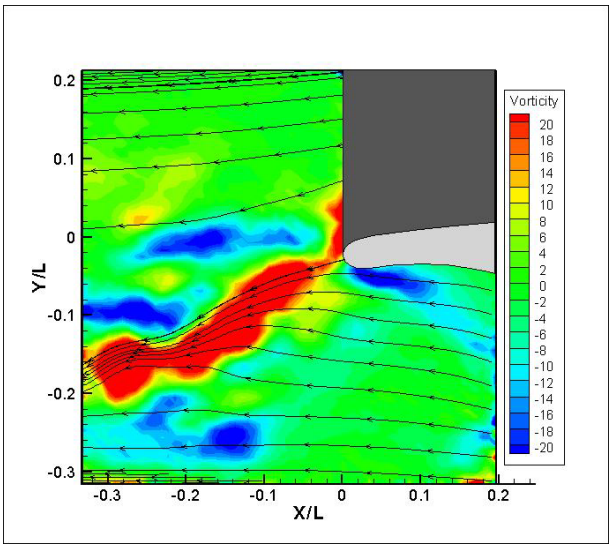

t = 0.54 sec

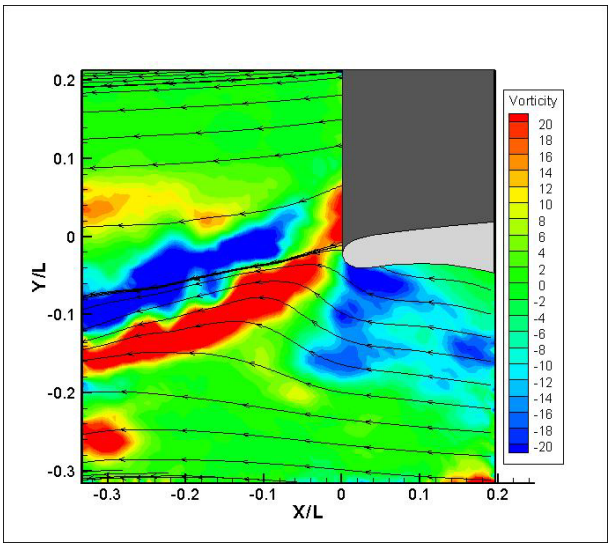

t = 0.72 sec

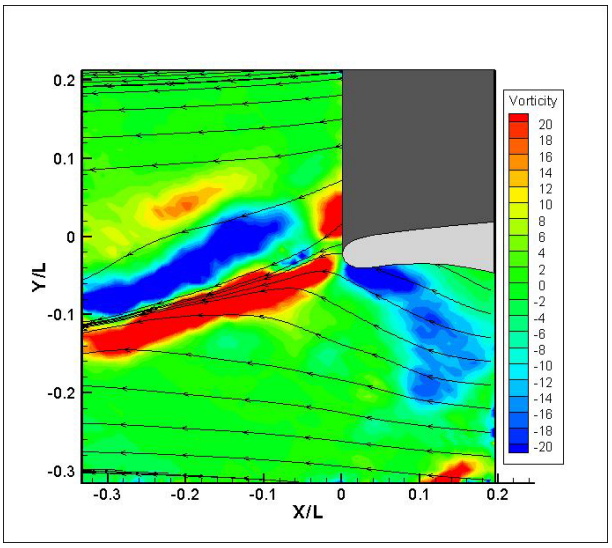

t = 1.00 sec

Figure 3.3.1.1 – Vorticity contours of time resolved results for the steady case of a momentum coefficient of 0.15

All six frames shown in Figure 3.3.1.1 illustrate clear consistency among the cases used (regardless of the time the frame corresponds to). That being said, the deflection angles of the streamlines vary from case to case. The frame corresponding to t = 0.36 sec shows an intersection point at Y/L = -0.11 whereas in the frame corresponding to t = 0.54 sec, the streamline intersects Y/L at -0.17. We can attribute this to the velocity fluctuation resulting from our jet.

3.3.2 Time Resolved Vorticity Distribution (Steady @ $C_\mu = 0.60$)

We repeat our procedure here for a momentum coefficient value of 0.60. Again, there is no driver frequency present.

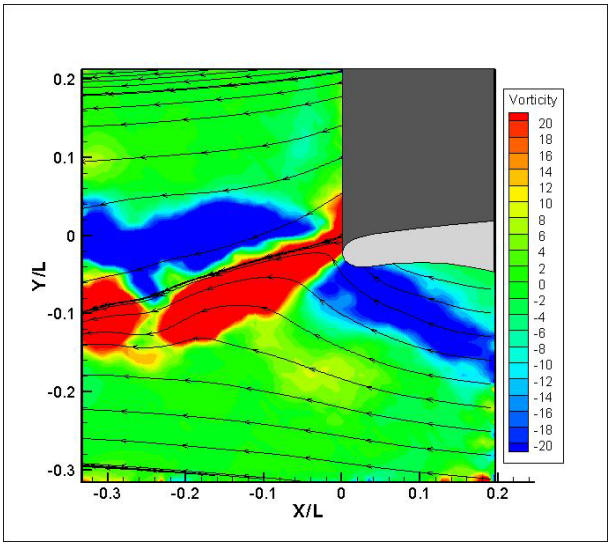

t = 0.00 sec

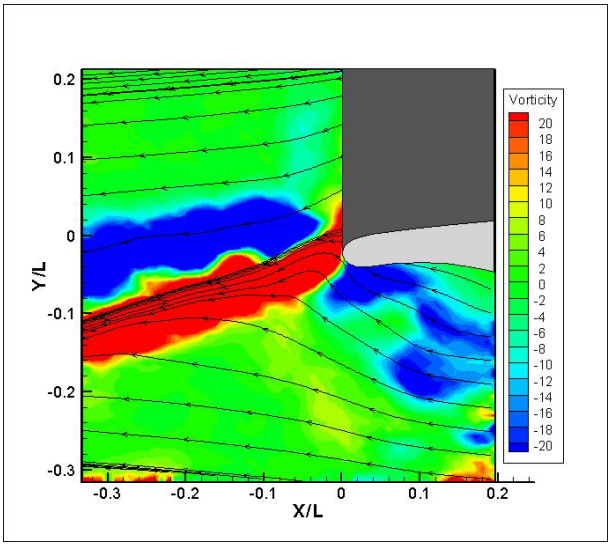

t = 0.18 sec

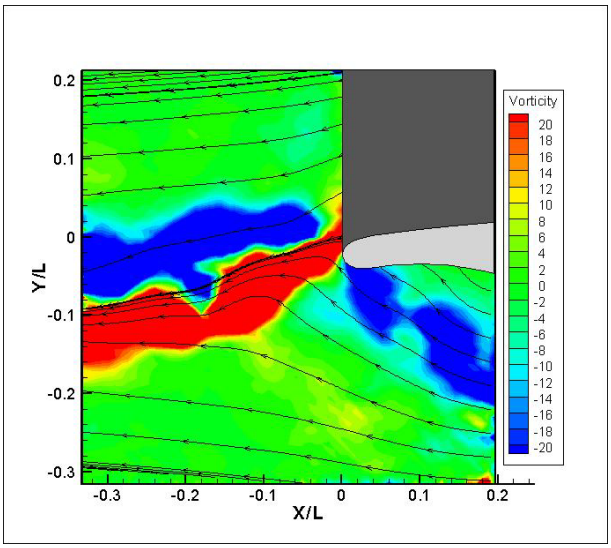

t = 0.36 sec

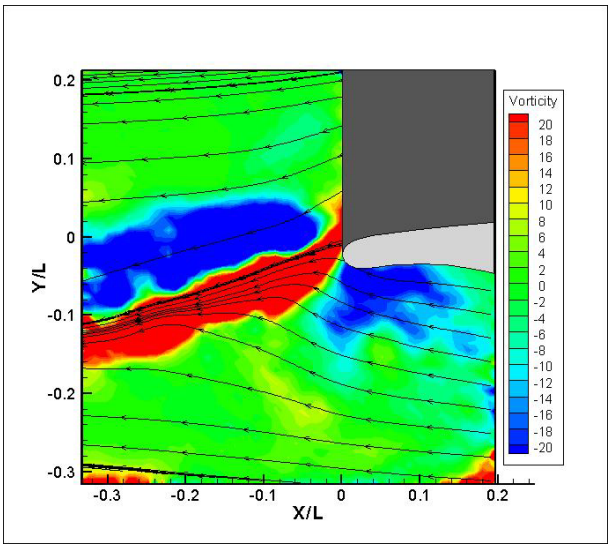

t = 0.54 sec

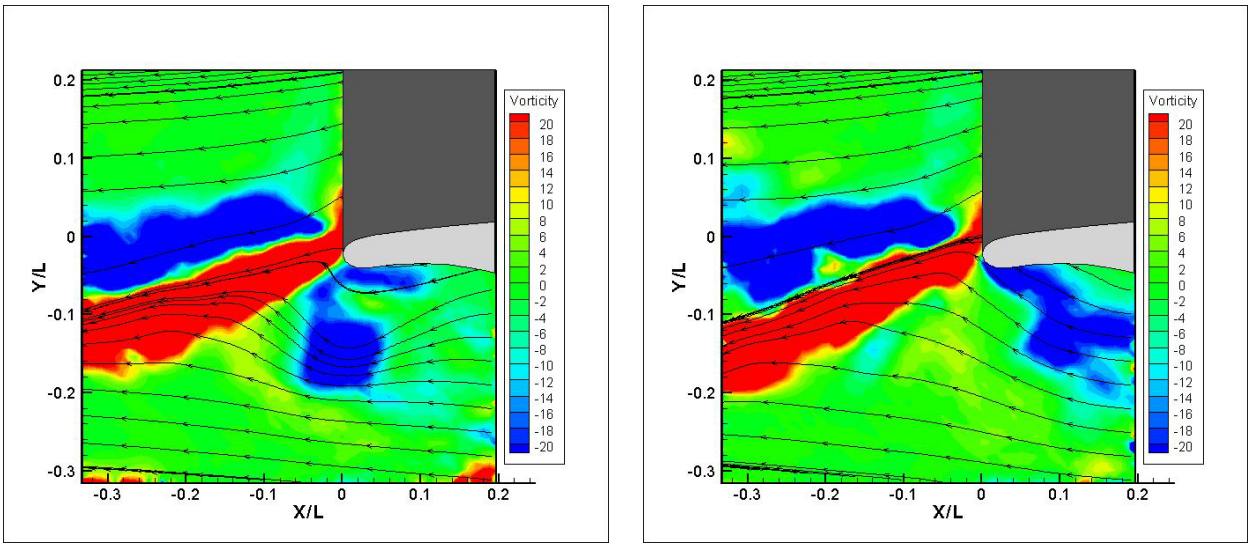

t = 0.81 sec t = 1.00 sec

Figure 3.3.2.1 – Vorticity contours of time resolved results for the steady case of a momentum coefficient of 0.60

Observe the uniformity in all six frames shown in Figure 3.3.2.1. Note also that each of the six frames presented is very similar to Figure 3.1.1.1 (c) which was the frame of the time-averaged case. This is consistent with our earlier observation that the individual frames in time-invariant flow are very coherent. Observe, however, that the deflection angles fluctuate from frame to frame. At t = 0.36 sec, we see that the intersection point at X/L = 0 is at Y/L = -0.1 whereas at t = 0.54 sec, it is at -0.12. Though the variation is small, there is still a presence of fluctuations in the jet. Note also that all of the areas in the vicinity of the jet have a presence of shear layers. As the angles of the streamlines resulting from the jet fluctuate, we see corresponding behavior in the shear layers as well. Recall from earlier discussions that we see an area of negative vorticity intersecting the airfoil at (X/L, Y/L) = (0, -0.04).

3.3.3 Time Resolved Vorticity Distribution (Steady @ $C_\mu = 2.68$)

Lastly, we will examine the highest momentum coefficient value ($C_\mu = 2.68$) for time-invariant flow.

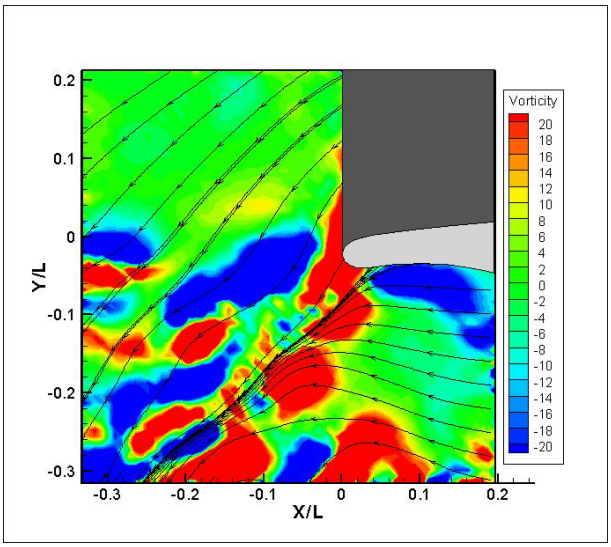

t = 0.00 sec

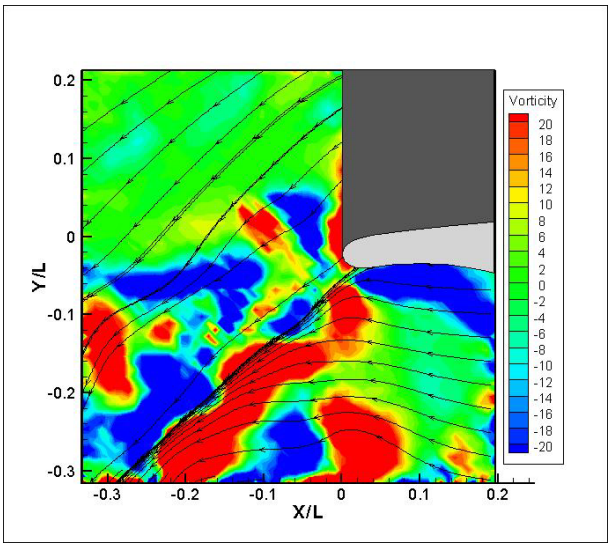

t = 0.18 sec

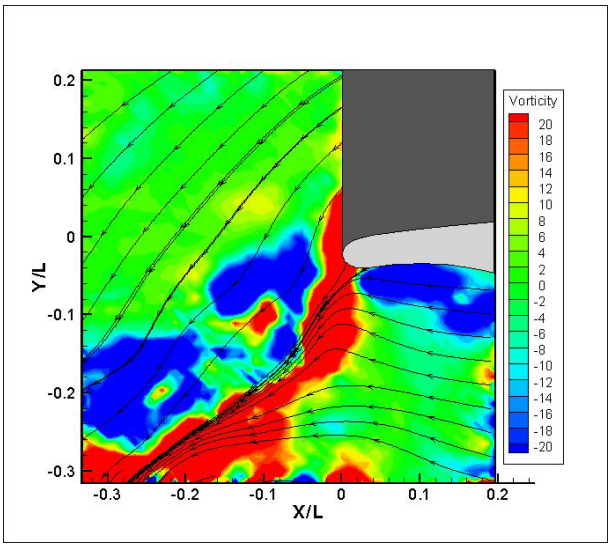

t = 0.36 sec

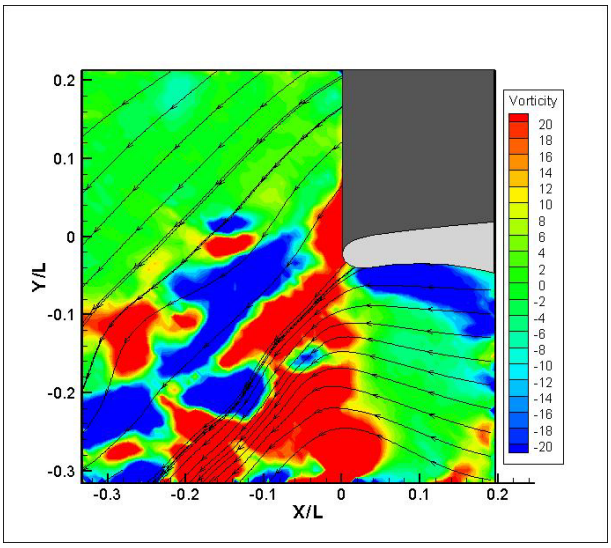

t = 0.54 sec

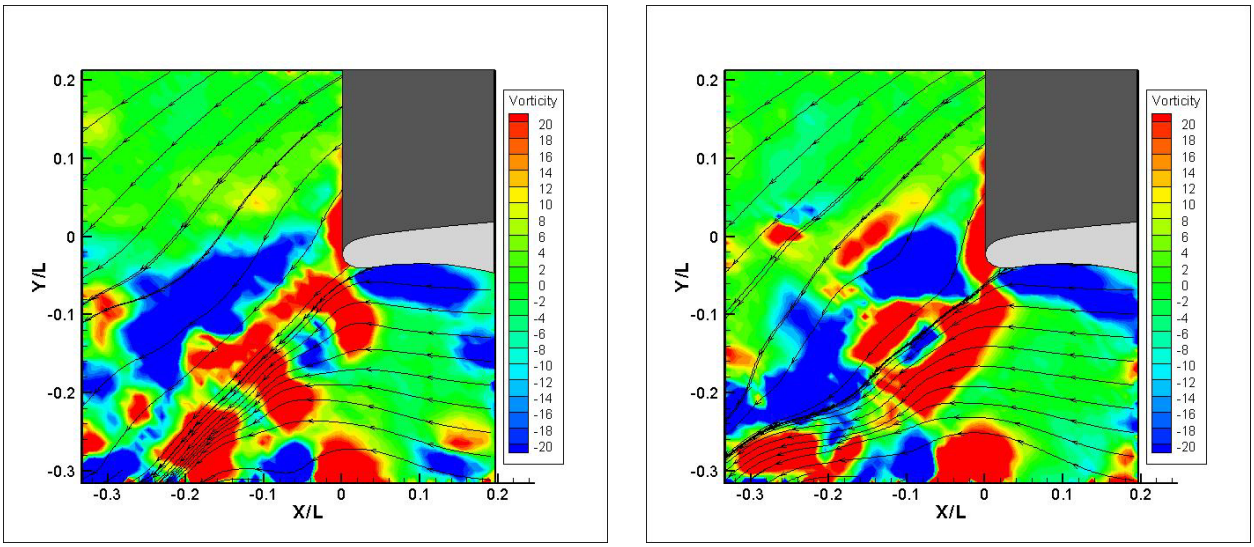

t = 0.81 sec t = 1.00 sec

Figure 3.3.3.1 – Vorticity contours of time resolved results for the steady case of a momentum coefficient of 2.68

All six frames shown in Figure 3.3.2.1 are similar to one another but what differs in this case is how our individual frames compare with the time averaged case shown in Figure 3.1.1.1 (f). Due to the fact that our value of momentum coefficient is about four times higher than the previous case i.e. (C_μ = 0.60), we can clearly observe greater regions of shear stress in the form of rapidly degenerating vortices in the immediate vicinity of the jet. These can be seen in the form of regions of positive (red) and negative (blue) vorticity on either side of the deflection angle. The time-averaged case, which is effectively the temporal mean of all 2000 frames, shows significantly different results. Figure 3.1.1.1 (f) shows an area of concentrated negative vorticity at (X/L, Y/L) = (-0.16, -0.08) and a corresponding region of positive vorticity at (X/L, Y/L) = (-0.06, -0.15). On the contrast, all frames illustrated in Figure 3.3.3.1 have regions of both positive and negative vorticity scattered in all X/L and Y/L locations less than 0.

3.3.4 Time Resolved Vorticity Distribution (Pulsed @ C_μ = 0.02)

We can now present our time-resolved results for the cases for which they are most effective. In the interest of avoiding redundancy stemming from the similarity in the fluid dynamics among these cases, every other case will be shown. Recall that in this case, a forced frequency is

present. An additional item of note is that each set of the unsteady cases has been synchronized such that the origin time, t = 0 sec, corresponds to the trough between the two complete cycles collected for study. The first case to be shown is the lowest non-zero value for time-variant flow.

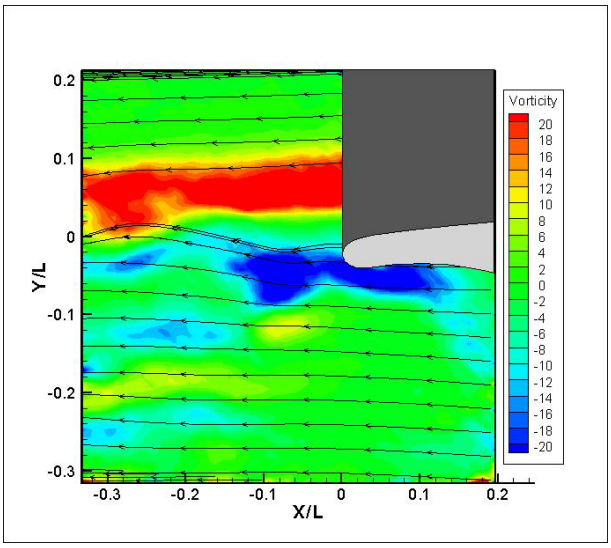

t = 0.00 sec

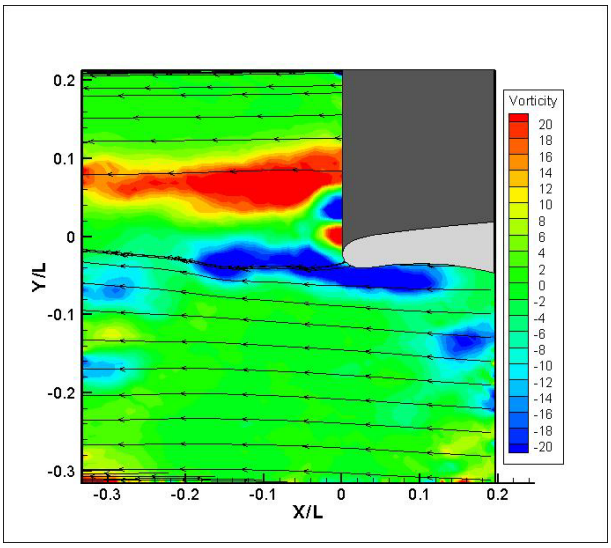

t = 0.14 sec

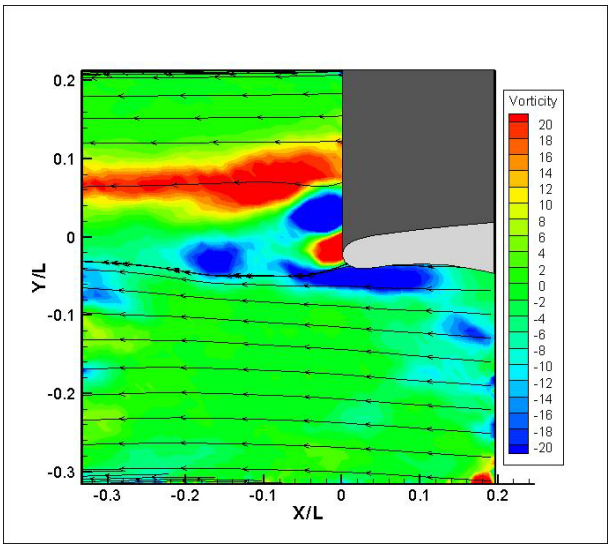

t = 0.16 sec

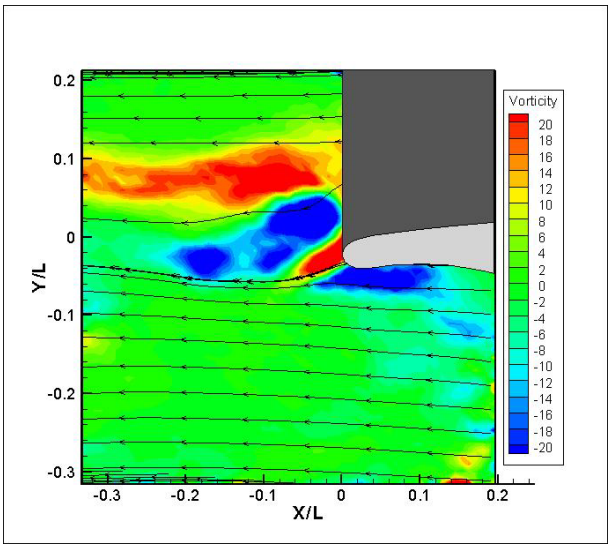

t = 0.26 sec

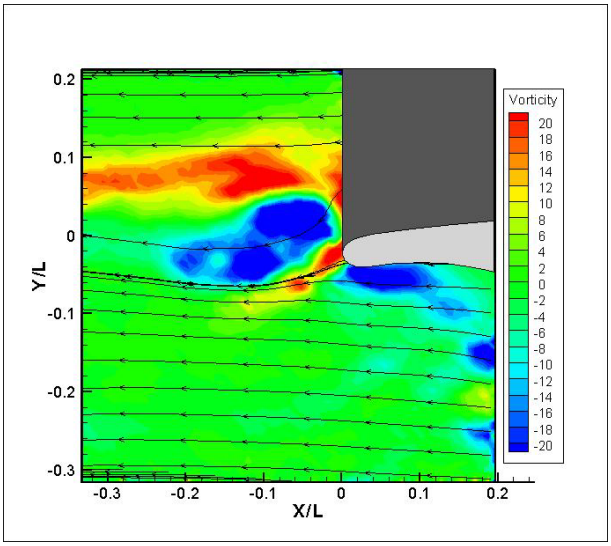

t = 0.36 sec

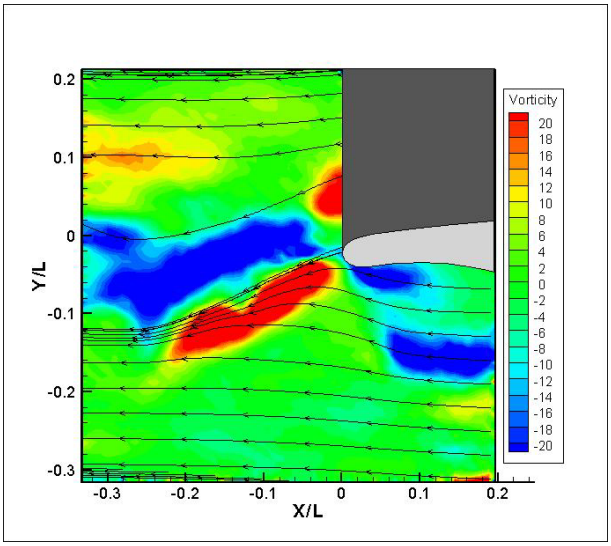

t = 0.50 sec

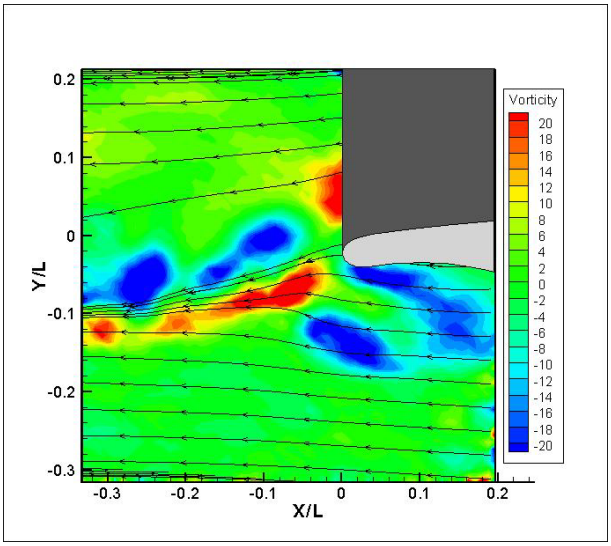

t = 0.60 sec

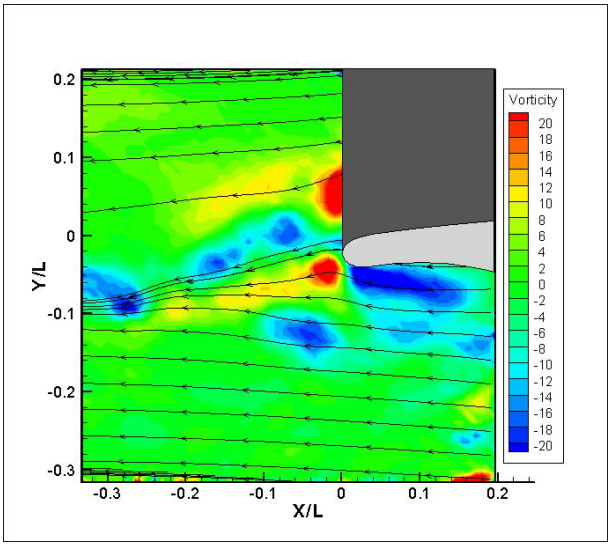

t = 0.65 sec

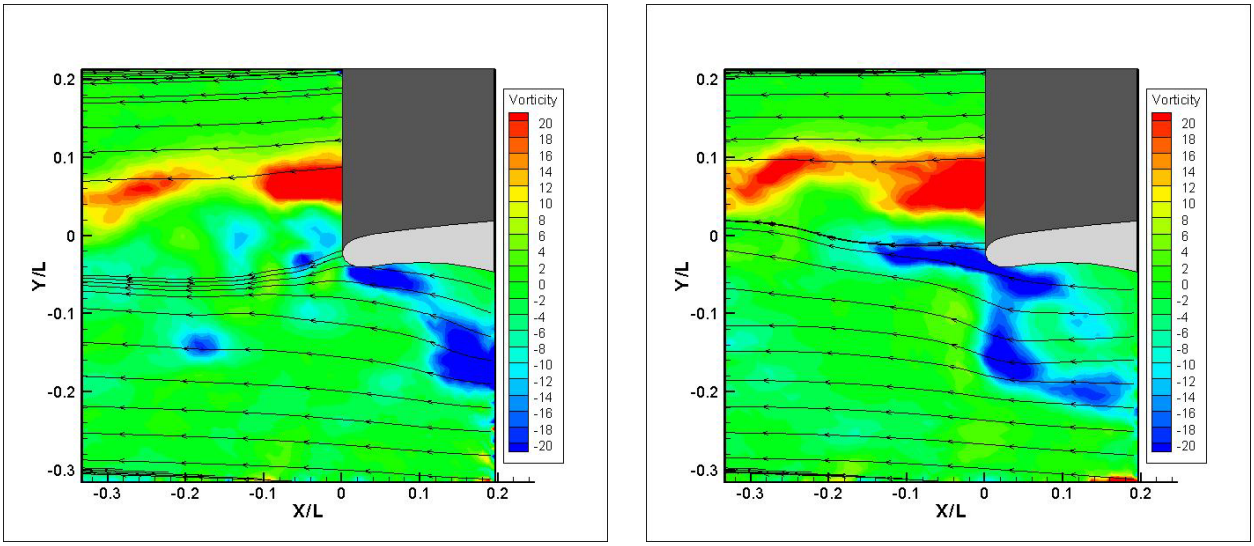

t = 0.75 sec t = 1.00 sec

Figure 3.3.4.1 – Vorticity contours of time resolved results for the pulsed case of a momentum coefficient of 0.02

Figure 3.3.4.1 provides us with substantial detail on the reversal of vorticity signs that was mentioned earlier. At t = 0, we can observe separated flow resulting from the lack of presence of a Coanda jet. At t = 0.14 sec, however, we can clearly see the formation of a vortex pair with the positive and negative vortices centered at (X/L, Y/L) = (0, 0) and (0, 0.05) respectively. Note that even in this short time interlude there is a clear reversal in the location of regions with negative and positive vorticity. Frames corresponding to t = 0.16 sec, t = 0.36 sec, and t = 0.50 sec effectively portray the same pair of vortices shown in the second frame at subsequent points in time. Note that we see intensification in strength as they move downstream. As expected, the temporal location of highest intensity is at the center of the cycle i.e. t = 0.50 sec. The last four frames (t = 0.60 sec to t = 1.00 sec) depict a gradual diminishing of vorticity.

3.3.5 Time Resolved Vorticity Distribution (Pulsed @ C_μ = 0.24)

We repeat our procedure here for a momentum coefficient value of 0.24 with a forced frequency.

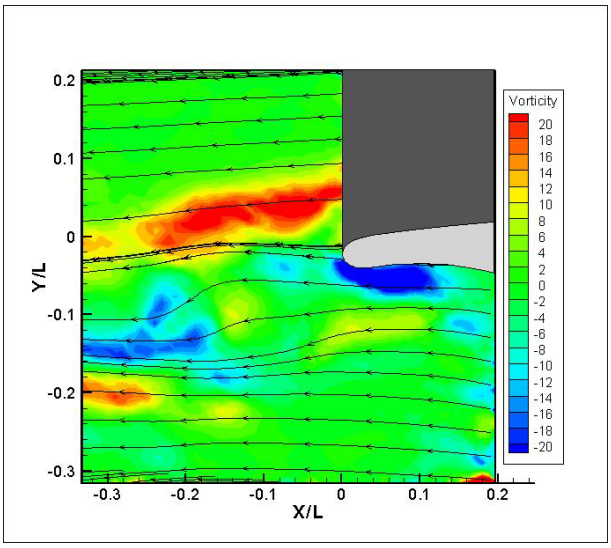

t = 0.00 sec

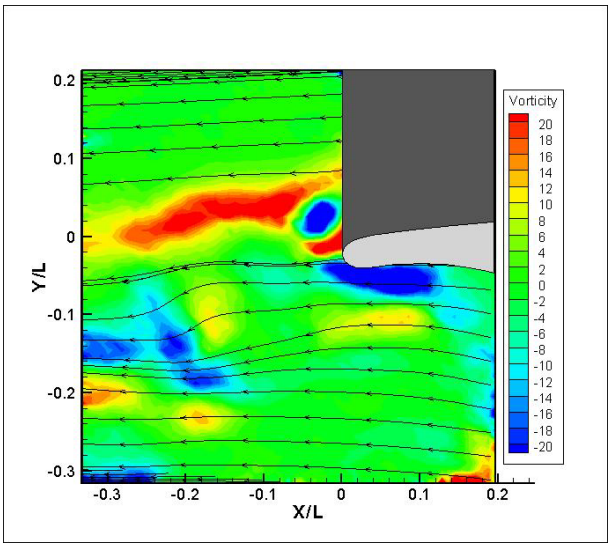

t = 0.09 sec

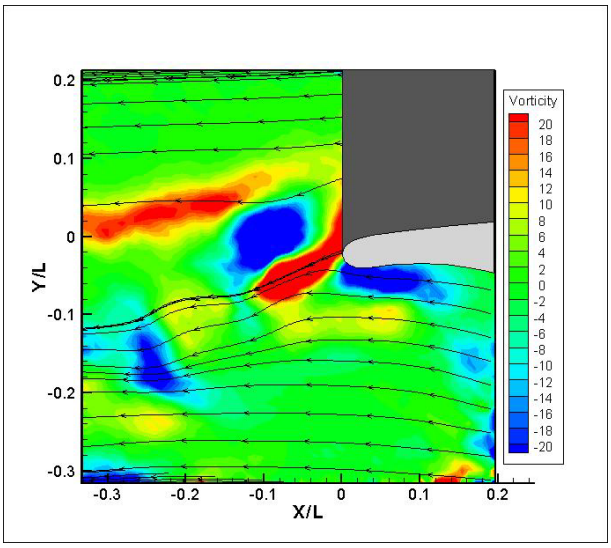

t = 0.20 sec

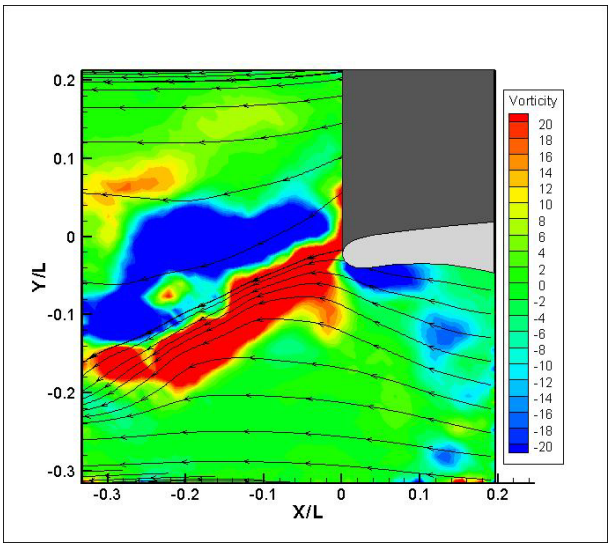

t = 0.31 sec

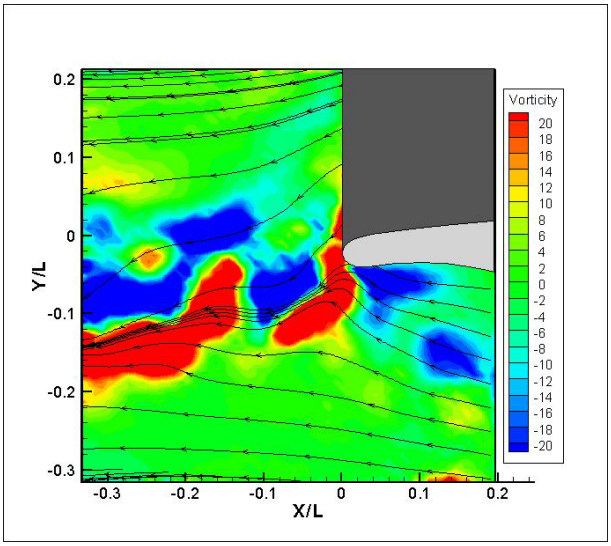

t = 0.44 sec

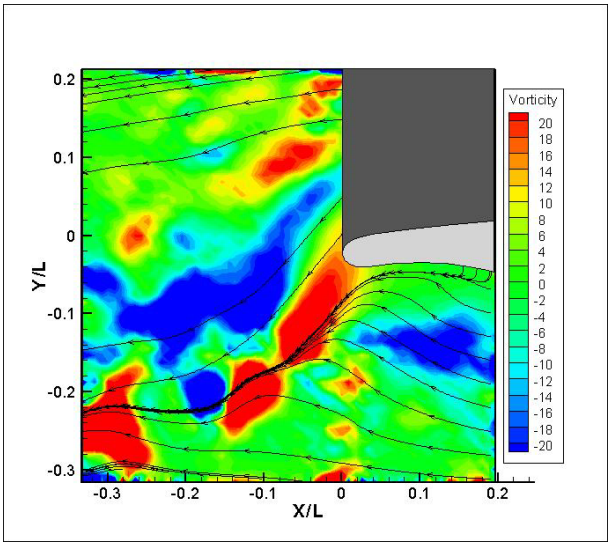

t = 0.47 sec

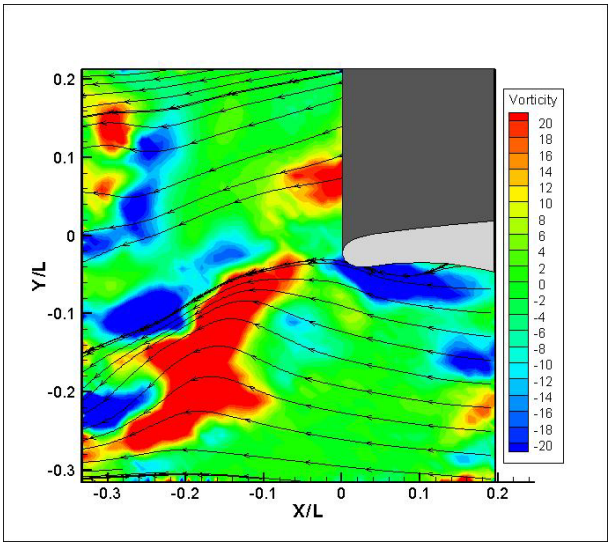

t = 0.65 sec

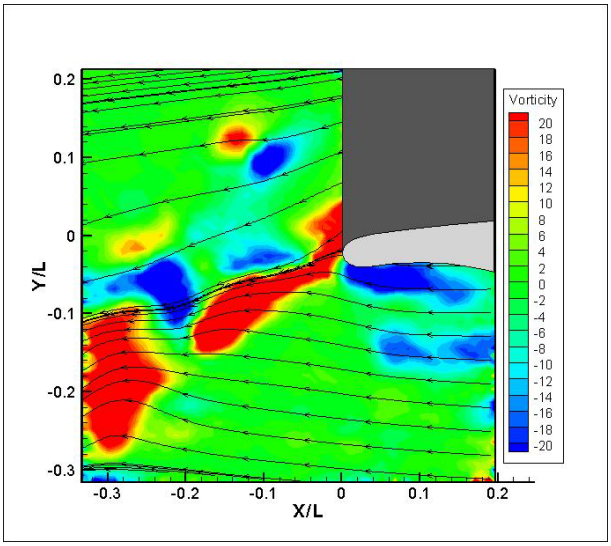

t = 0.75 sec

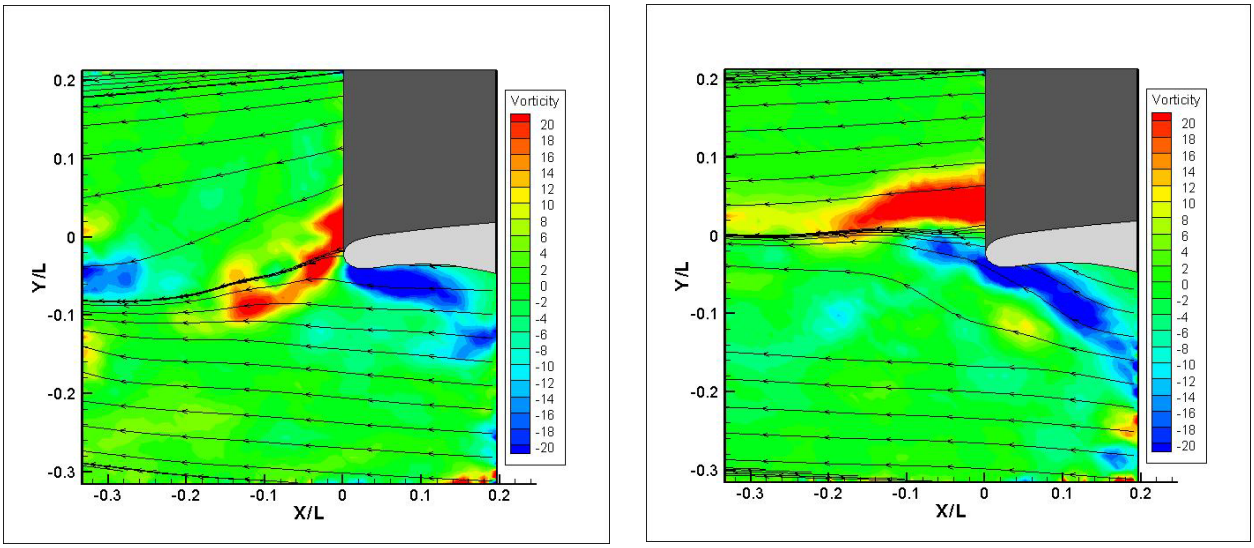

t = 0.87 sec t = 1.00 sec

Figure 3.3.5.1 – Vorticity contours of time resolved results for the pulsed case of a momentum coefficient of 0.24

The first observation that stands out is that at locations in time near the peak of the cycle, (see t = 0.47 sec), we can see an widespread intensification in the vorticity magnitude. In the first frames, we see a coherent region of positive vorticity at (-0.1, 0.04). Observing the frame corresponding to t = 0.47 sec, on the other hand, does not show a coherent pattern of two vortices (one positive and one negative). Rather, we see a number of areas with vortex breakdown which we can attribute to areas of high shear stress layers. There is, however, a dominant region of negative vorticity centered at (-0.15, -0.1) and a positive region centered at (-0.04, -0.1). What we also observe is that in this frame, the streamlines are spaced wider apart than in the other frames.

3.3.6 Time Resolved Vorticity Distribution (Pulsed @ $C_\mu = 0.60$)

What will be presented next is the highest momentum value for the time-variant case. Note that the same value was discussed earlier for the steady case. We will go back to these two cases for an isolated study in the next section.

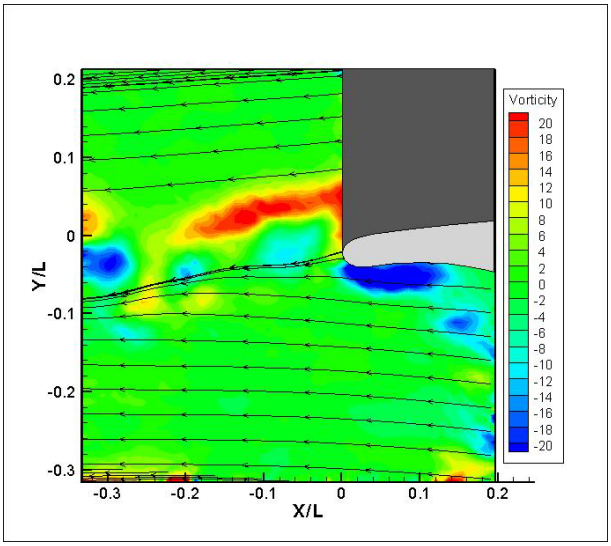

t = 0.00 sec

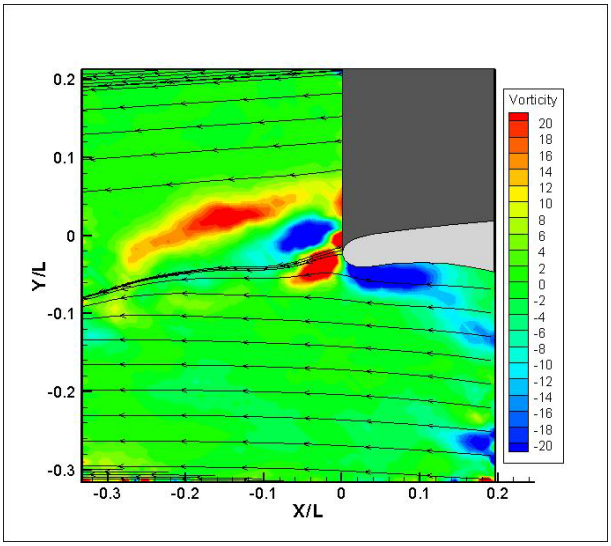

t = 0.04 sec

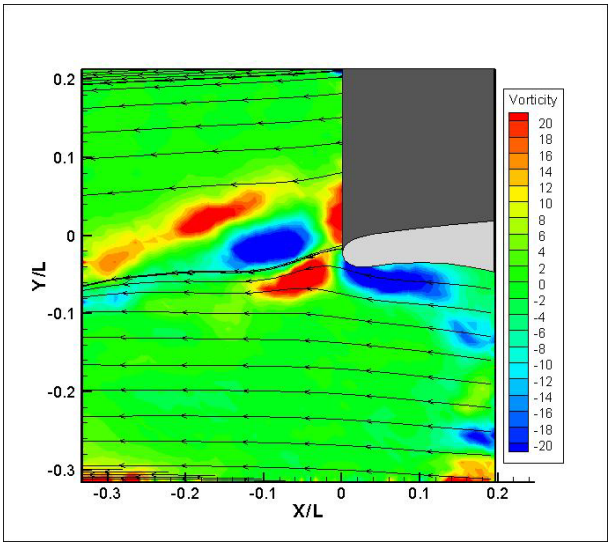

t = 0.07 sec

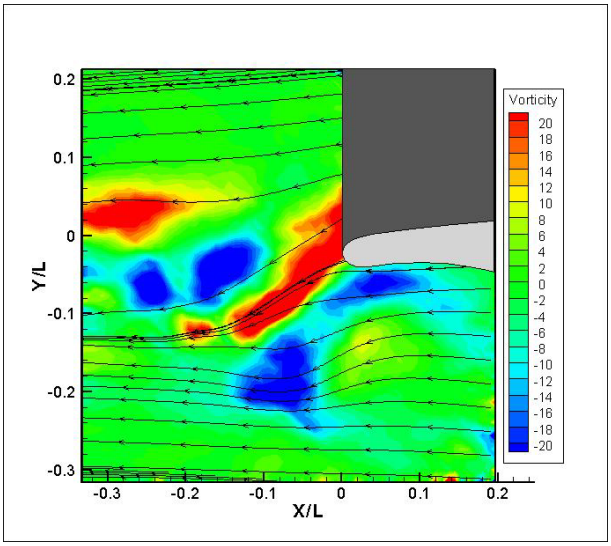

t = 0.12 sec

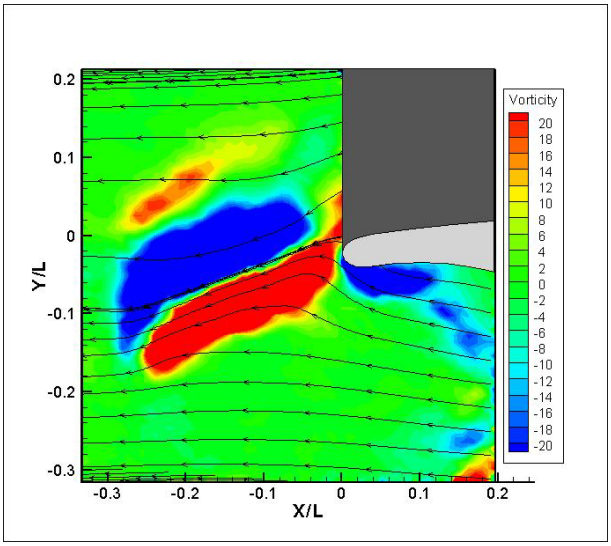

t = 0.20 sec

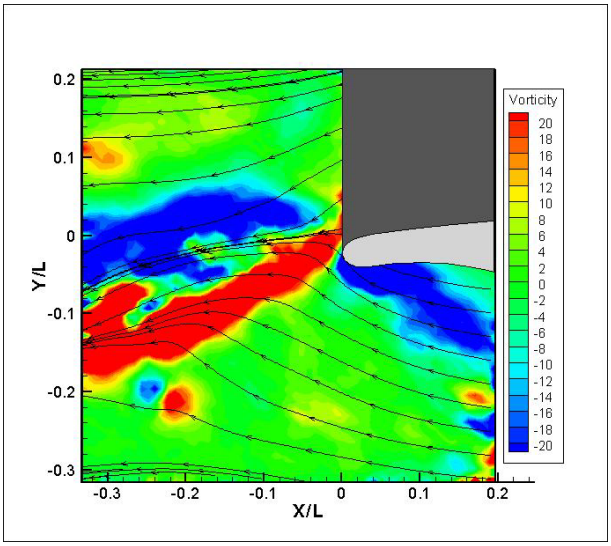

t = 0.35 sec

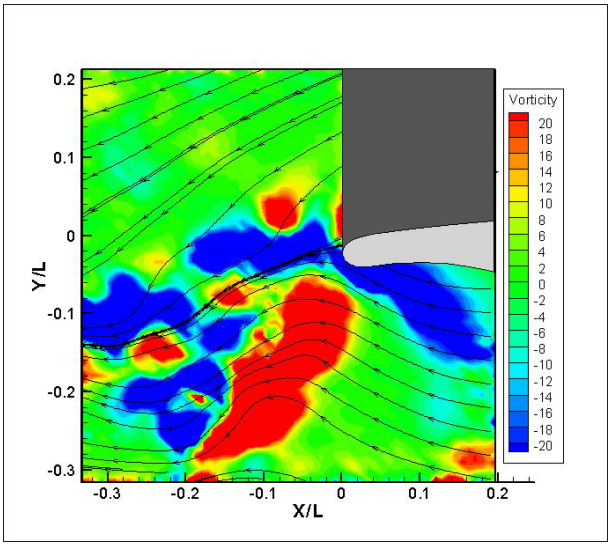

t = 0.49 sec

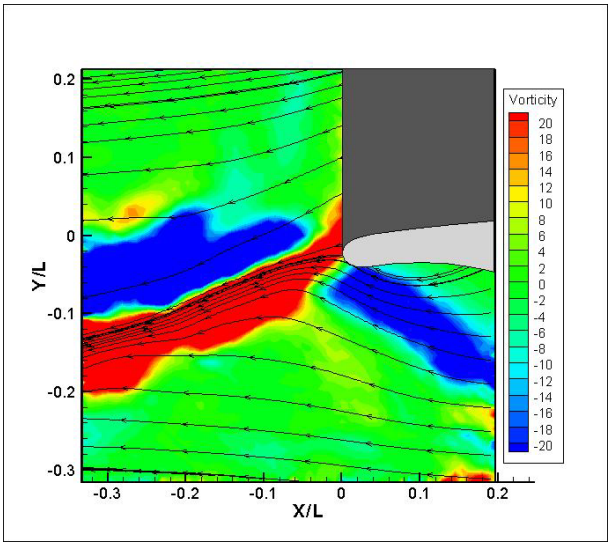

t = 0.55 sec

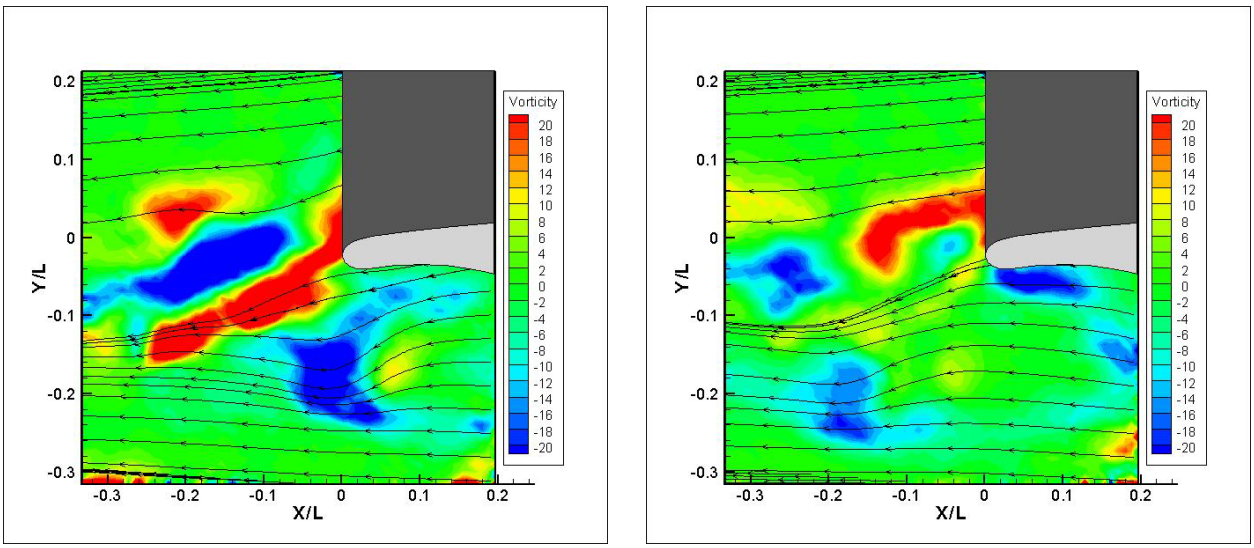

t = 0.70 sec t = 0.95 sec

Figure 3.3.6.1 – Vorticity contours of time resolved results for the pulsed case of a momentum coefficient of 0.60

A number of traits in the flow dynamics for the highest momentum coefficient case show up distinctly from the previous case. The curvature we see in the streamline shape at t = 0.12 is primarily driven by the clockwise angular velocity component contributed by the vortex centered at (X/L, Y/L) = (-0.14, -0.05). Also note that at t = 0.49 sec (peak of the cycle), we see a rapid breakdown for vortices generated from the pneumatic jet. Lastly, in frames t = 0.20 sec to t = 0.49 sec, we see a gradual intensification of the area of negative vorticity at the pressure side of the Coanda surface centered at approximately (-0.05, -0.05).

3.3.7 Time Resolved Vorticity Distribution for $C_\mu = 0.60$

As was done with the time-averaged results, we will repeat our cases of contrasting reduced frequency values at a constant momentum coefficient. In an attempt to portray our results in a more concise manner, the author will refer to the frames already presented in this chapter.

The primary difference between the dynamics of the flow corresponding to these two cases lies in the shape of the streamline. Due to the close proximity of the regions of positive and negative vorticity in Frame 3.3.2.1, we do not see the curvature that was present at t = 0.12 sec in

Figure 3.3.6.1. Also, the rapid breakdown of vortices that we see at t = 0.49 sec in the latter figure is not present in the time-invariant flow. Note that this observation is a little unexpected because the momentum coefficient for the unsteady case is defined to be that corresponding to the peak of the cycle. Our intuition therefore tells us that the flow physics at the peak of the pulsed cycle should be similar to those for the steady case (any frame), yet it is quite evident that the dynamics of the jet play a significant role in shaping flow characteristics.

CHAPTER 4

4 DISCUSSION

4.1 Introduction

Both the Tecplot® images as well as the vorticity spectra presented in the previous chapter provide us with valuable insight into the flow dynamics aft of the Coanda surface. A number of characteristics of the flow were independent of the forced frequency whereas it was clear by the velocity spectra that others were strongly influenced by the forced frequency. In an attempt to further expand on our knowledge of Coanda jet flow dynamics, the authors will devote this section to an explanation of the flow physics.

4.2 Time Averaged Vorticity Distribution

Recall that we pointed out the reversal of vorticity sign as one of the effects of the application of a pneumatic jet. When a Coanda jet is not applied, we see that the direction of angular velocity on each side of the airfoil is that of separated flow such as that over a stationary circular cylinder. The Strouhal Number at which the vortices shed (based on our MATLAB® images) is consistent with that which would observe for flow over a circular cylinder for which the St was based on the diameter i.e. thickness ($St \approx 0.3$). This is predominantly due to the fact that the primary velocity fluctuations for this flow case correspond to the shedding frequency over the airfoil. The thickness of the airfoil combined with the high camber and the rounded trailing edge will all contribute to determining the Strouhal Number for velocity fluctuations which are driven by the frequency of vortex shedding.

We also found that the interaction of the Coanda jet reverses the signs on the angular velocity. Essentially, what is taking place is a change in the velocity profile such that the profiles remain symmetric but a large component of velocity is adjoined at the center. The region on either side of the jet contribution is effectively a cavity that has properties similar to the boundary layer. However, due to the fact that each region is essentially symmetric reflection of the other, we see opposite signs as illustrated in Figure 4.2.1. Bear in mind that the magnitude of the Coanda jet will determine the location and shape of the center region in the velocity profile as a high value of momentum coefficient will act to move the vortices closer to the pressure side of the airfoil.

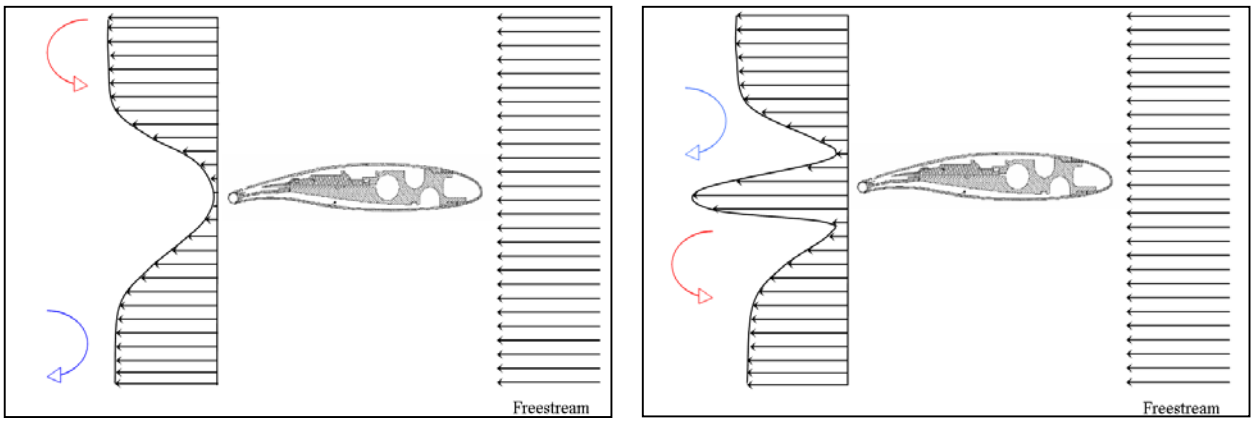

Figure 4.2.1 – Velocity profiles of flow downstream of CCW with Coanda Jet inactive (left) and active (right)

4.3 Time Averaged Velocity Spectra

Within the six frames corresponding to the steady Coanda jets, we see a clear distinction in the dominant Strouhal Number values in Figure 3.2.1.2. Observe that in frames (a) through (c), the regions of maximum intensity correspond to St ≈ 0.3. The Strouhal Number for vortices shedding from a stationary circular cylinder (based on diameter) is approximately 0.2. This suggests that the predominant Strouhal Number value for low momentum coefficients is governed by a typical bluff body vortex shedding behavior. Frames (d) through (f), however, reveal the presence of a secondary frequency corresponding to a Strouhal Number value St ≈ 1.0. Taking into consideration that this value presents itself only when a high region of shear stress resulting from the jet is present as well as the fact that this value is consistent with the value of Strouhal Number corresponding to shear stress instabilities, we can conclusively state that the secondary regions of velocity fluctuation are from separation in the shear layer. Also observe that in frame (f) of Figure 3.2.2.1, we see an intensification of the regions corresponding to this value. This implies that for a given momentum coefficient, a pulsed jet intensifies the breakdown of shear stress layers at a more rapid rate than its steady counterpart.

4.4 Time Resolved Vorticity Distribution

The primary advantage in the DPIV system used in the current work is the ability to look at variations in flow dynamics resulting from the application of a time-invariant jet. We presented our results for this case in a frame-by-frame fashion in the previous chapter. Recall that regions corresponding to the peak of a cycle had larger deflection angles associated with them (see frame corresponding to t = 0.50 sec in Figure 3.3.4.1). A secondary, though equally important, observation was that higher values of C_μ also contribute to greater circulation. At t = 0.55 sec in Figure 3.3.5.1, we can see that the location of intersection between the streamlines at the jet and the Coanda surface move upstream. Recall from Chapter 1 that this has a direct effect in amplifying lift which validates our theory that higher values of momentum coefficient will directly contribute to the net force on the airfoil. The direction in which the flow moves over the trailing edge as a result of the Coanda jet is in the opposite direction (counter-clockwise) of the arriving wake. However, because the flow can only move a certain distance upstream before it is forced in the direction of the incoming flow, there forms a region where the angular velocity is negative, the same as the wake from upstream. This contributes to the intensity of the region of negative vorticity and we clearly see this during the peak of the cycles.

CHAPTER 5

5 CONCLUSIONS

5.1 Conclusions

By using a spatio-temporal non-invasive flow measurement technique, a great deal of insight was developed with regards to flow at the trailing edge of a Coanda airfoil. The presentation of our data with Tecplot® and by developing a MATLAB® code, we found a number of revealing items about this unconventional flow.

One of the first items to be noted was the direction of angular velocity in areas of vorticity for cases of separated flow relative to those with attached flow. It was demonstrated that the presence of a Coanda jet significantly alters the velocity profile and hence the location of areas of vorticity. It was also found that at higher values of C_μ, we see a greater deflection angles in the streamlines which validates our hypothesis that one of the impacts of the Coanda jet is a change in the pressure difference on the two surfaces. Additionally, we see that higher momentum coefficients results in greater circulation as manifested by the location at which the streamlines meet the airfoil. The greater circulation around the Coanda surface that is made at higher momentum coefficient values is in the same direction as the arriving wake thereby amplifying its magnitude.

From the results obtained from our spectra, we see two primary differences. Firstly, in the case of a pulsed jet, there is the presence of a second weaker vortex that has a Strouhal Number that is three times greater. Secondly, the vortices resulting from the jet take significantly longer to disseminate.

CHAPTER 6

6 FUTURE WORK

6.1 Future Work

The present work makes a significant contribution to our understanding of flow behavior resulting from a Circulation Control device such as a Coanda jet. By using Digital Particle Image Velocimetry, the author was able to analyze the flow behavior by non-invasive means. Despite the gain in knowledge that was a result of this work, a number of questions still remain unanswered with regards to the flow physics and future work will be necessary to fill in this gap.

Due to hardware limitations, only two non-dimensional frequencies were analyzed. Work by other authors, namely Jones et al., suggests that lift can be optimized at a Strouhal number of 35. Due to the fact that this dimensionless frequency is an order of magnitude higher than the one in the current work, there is a strong possibility that the resulting flow behavior, in particular the forced shedding frequency, will be different. At the time this work was completed, the author was not aware of any work that makes an effort to analyze the flow at such high Strouhal Numbers. Additionally, hardware limitations were the driving factor in constraining the author to one duty cycle i.e. 50%. Though contemporary work in this area of aerodynamics highlights the benefits at various duty cycles, the current contribution does not utilize the variation of this parameter. The authors strongly feels that further analysis at different duty cycles could yield variable insight into vortex shedding behavior.

It was also noted in the work that there is significant vorticity component that is contributed from flow upstream. There is reason to believe that this is a result of leading edge flow separation but this could not be verified independently. A useful contribution could take the form of data sampling and analysis at the leading edge for the conditions that were employed for this particular work to validate or annul this hypothesis. Additionally, due to the orientation of the airfoil, flow behavior on the suction side could not be analyzed. By placing the airfoil at the same angle of attack but with reversed orientation, considerable gains could be made in what is known about the flow on the opposite surface, particularly at the trailing edge jet slot.

An additional item to note was that only the zero lift angle of attack was utilized. Hence any lift component that was present was due to the Coanda jet alone. A variety of angles of

attack could be used to further examine the effect of pneumatic jet flow on the lift characteristics. Also, recall that only the slot at the suction side was used as this is conductive to a high lift setting. One could also explore the effect of using the opposite slot or the combination of the two to explore the flow physics for dynamically variant momentum coefficients.

REFERENCES

Abiven, C., Vlachos, P. P., (2002). "Super spatio-temporal resolution, digital PIV system for multi-phase flows with phase differentiation and simultaneous shape and size quantification", Int. Mech. Eng. Congress, Nov. 17-22, 2002, New Orleans, LA

Abramson, J., and Rogers E. O., "High Speed Characteristics of Circulation Control Airfoils," AIAA Paper 1983-0265

Amitay, Michael, Honohan, Andrew, Trautman, Mark, Glezer, Ari, (1997). "Modification of the Aerodynamic Characteristics of Bluff Bodies Using Fluidic Actuators", AIAA Paper 1997-2004

Amitay M, Smith B. L. and Glezer, (1998). "Aerodynamic flow control using synthetic jet technology", AIAA Paper 1998-0208

Amitay, M., Pitt, D., Kibens, V., Parekh, D., Glezer, A., (2000). "Control of Internal Flow Separation Using Synthetic Jet Actuators", AIAA Paper 2000-0903

Amitay, M., Horvath, M., Michaux, M., Glezer, A., (2001). "Virtual Aerodynamic Shape Modification at Low Angles of Attack using Synthetic Jet Actuators", AIAA Paper 2001-2975

Amitay, Michael, Smith, Douglas R., Vibens, Valdis, Parekh, David E., Glezer, Ari, (2001). "Aerodynamic Flow Control over an Unconventional Airfoil Using Synthetic Jet Actuators", AIAA Journal Paper Vol. 39, No. 3, March 2001

Amitay, Michael, Glezer, Ari, (2002). "Role of Actuation Frequency in Controlled Flow Reattachment over a Stalled Airfoil", AIAA Journal of Aircraft Vol. 40, No. 2, February 2002

Asami, Kengo, Sawada, Keisuke, (1996). "Numerical study on the underexpanded Coanda jet", AIAA Fluid Dynamics Conference, 27th, New Orleans, LA, June 17-20, 1996

Bradley, L.C., Franke, M.E., (1997). "An experimental investigation of a sting-mounted circulation control wing", AIAA Paper 1997-0035

Burrin, R.R., Ahuja, K.K., Saliuddin, M. (1987). "High speed flight effects on noise propagation", Aerospace Sciences Meeting, 25th, Reno, NV, Jan 12-15, 1987

Cagle, Christopher M., Jones, Gregory S., (2002). "A Wind Tunnel Model to Explore Unsteady Circulation Control for General Aviation Applications", AIAA Paper 2002-3240

Carter, C.J., Guillot, S.A., Ng, W.F., Copenhaver, W.W., (2001). "Aerodynamic Performance of a High-Turning Compressor Stator with Flow Control", AIAA Paper 2001-3973

Chambers, F.W., Jones, G.S., (2001). "Density and Mach Number Effects on Piezoelectric Flow Control Actuator Performance", AIAA Paper 2001-3025

Englar, Robert J., and Williams, R. M., "Design of a Circulation Control Stern Plane for Submarine Applications," NSRDC, TN AL-200, March 1971.

Englar, Robert J., "Circulation Control Pneumatic Aerodynamics: Blown Force and Moment Augmentation and Modification; Past, Present & Future," AIAA Paper 2000-2541

Englar, Robert J., Campbell, Bryan A., (2002). "Development of Pneumatic Channel Wing Powered-Lift Advanced Super-Stol Aircraft", AIAA Paper 2002-2929

Fleming, Jon, Olcman, Semih, Burdisso, Ricardo, Ng, Wing, (2004). "Sensing for Active Flow Control in Advanced Propulsion-Airframe Integration Systems", 42nd AIAA Aerospace Sciences Meeting and Exhibit 5-8 January 2004, Reno, Nevada

Gad-el-Hak, Mohamed, (2001). "Flow Control: The Future", AIAA Journal of Aircraft Paper Vol. 38, No. 3, May-June 2001

Grossman, K.R., Cybyk, B.Z., VanWie, D.M., (2003). "Sparkjet Actuators for Flow Control", 41st Aerospace Sciences Meeting and Exhibit 6-9 January 2003, Reno, Nevada

Hassan, Ahmed A., (2001). "Applications of Zero-Net-Mass Jets for Enhanced Rotorcraft Aerodynamic Performance", AIAA Journal of Aircraft Vol. 38, No. 3, May-June 2001

Hites, Michael, Nagib, Hassan, Wark, Candance, (1997). "Velocity and wall shear-stress measurements in high-Reynolds-number turbulent boundary layers", AIAA Paper 1997-1873

Hites, Michael, Nagib, Hassan, Bachar, Tomer, Wygnanski, Israel, (2001). "Enhanced Performance of Airfoils at Moderate Mach Numbers Using Zero-Mass Flux Pulsed Blowing" AIAA Paper 2001

Honohan, Andrew M., Amitay, Michael, Glezer, Ari, (2000). "Aerodynamic Control using Synthetic Jets", AIAA Paper 2000-2401

Imber, R. D., and Rogers, Ernest O., "Investigation of a Circular Planform Wing with Tangential Fluid Ejection," AIAA Paper 1996-0558

Jones, Gregory, Viken, S.A., Washburn, A.E., Jenkins, L.N., Cagle, C.M., (2002). "An Active Flow Control Concept for General Aviation Aircraft Applications", AIAA Paper 2002-3157

Joslin, Ronald D., Horta, Lucas G., Chen, Fang-Jenq, (1999). "Transitioning Active Flow Control to Applications", 30th AIAA Fluid Dynamics Conference, Norfolk, VA/28 June-1 July, 1999

Joslin, Ronald D., Viken, Sally A., (2001). "Aerodynamic performance of an active flow control configuration using unstructured-grid RANS", "Aerospace Sciences Meeting and Exhibit, 39th, Reno, NV, Jan. 8-11, 2001

Kim, H.D., Raghunathan, S., Setoguchi, T., Matsuo, S., (2000). "Experimental and Numerical Studies of Supersonic Coanda Wall Jets", AIAA Paper 2000-1814

Liu, Yi, Sankar, Lakshmi N., Englar, Robert J., Ahuja, Krishan K., Gaeta, R., (2004). "Computational Evaluation of the Steady and Pulsed Jet Effects on the Performance of a Circulation Control Wing Section", 42nd AIAA Aerospace Sciences Meeting and Exhibit 5-8 January 2004, Reno, Nevada

Mavris, Dimitri, Kirby, Michelle R., (1999). "Takeoff/Landing Assessment of an HSCT with Pneumatic Lift Augmentation", AIAA Paper 1999-0534

McQuilling, Mark, Jacob, Jamey, (2003). "A Comparative Study Between Ejector Nozzle and Vortex Generator Jet Flow Control Methods on a Low Pressure Turbine Blade Cascade Model", AIAA Paper 2003-4159

Medoza, J.M., Ahuja, K.K., (1996). "Cavity noise control through upstream mass injection from a Coanda surface", AIAA and CEAS, Aeroacoustics Conference, 2nd, State College, PA, May 6-8, 1996

Mitchell, Anthony M., Molton, Pascal, Barberis, Didier, Délery, Jean, (1999). "Control of Leading-Edge Vortex Breakdown by Trailing Edge Injection", AIAA Paper 1999-3202

Modi, V.J., Mokhtarian, F., Yokomizo, T., (1988). "Rotating air scoop as airfoil boundary-layer control", AIAA Journal of Aircraft Vol. 25 No. 10

Munday, David, Jacob, Jamey, Huang, George, (2002). "Active Flow Control of Separation on a Wing with Oscillatory Camber", AIAA Paper 2002-0413

Prandtl, L., (1904). "Über Flüssigkeitbewegung bei sehr kleiner Reibung", Verhandlugen des III. Internatinalen Mathematiker-Kongres (Heidelberg) pp. 484-491, 1905

Rogers, Ernest O., Donnelly, Martin J., (2004). "Characteristics of a Dual-Slotted Circulation Control Wing of Low Aspect Ratio Intended for Naval Hydrodynamic Applications", AIAA Paper 2004-1244

Seifert, Avi, La Tunia, G., (2000). "Separation Control at Flight Reynolds numbers: Lessons learned and Future directions", AIAA Paper 2000-2542

Sellers, William L., Jones, Gregory S., Moore, Mark D., (2002). "Flow Control Research at NASA Langley in Support of High-Lift Augmentation", AIAA Paper 2002-6006

Urzynicok, F., Fernholz, H., (2002). "Flow-Induced Acoustic Resonators for Separation Control", 1st Flow Control Conference, St. Louis, Missouri, June 24-26, 2002

Wu, Jingshu, Sankar, Lakshmi N., Kondor, Shayne, (2004). "Numerical Modeling of Coanda Jet Controlled Nacelle Configurations", 42nd AIAA Aerospace Sciences Meeting and Exhibit 5-8 January 2004, Reno, Nevada

VITA

Mian M. Hussain was born on November 12, 1981 near Islamabad, Pakistan. In 1986, his family moved to the United States where he spent the next four years. In 1990, they moved back to Islamabad and it is there that he completed high school. He enrolled in the Department of Aerospace and Ocean Engineering at Virginia Tech in August, 1999 where he received his Bachelors of Science degree in Aerospace Engineering in May, 2003. Upon the completion of his undergraduate curriculum, he entered graduate school in the Department of Mechanical Engineering at Virginia Tech where he successfully defended his M.S. degree in Mechanical Engineering with a concentration in Aerodynamics on December 15th, 2004. At the culmination of this work, he will be relocating to Seattle, WA to work for The Boeing Company. His initial work will be in the High Lift Aerodynamics Configuration Group for the Boeing 7E7.

"Ut Prosim"